International Journal of Biological Macromolecules 279 (2024) 135116

Contents lists available at ScienceDirect

International Journal of Biological Macromolecules

journal homepage: www.elsevier.com/locate/ijbiomac

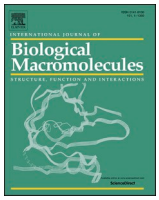

# Extraction, purification, chemical characterization, and in vitro hypoglycemic activity of polysaccharides derived from *Rosa laevigata* Michx.

Shuai Chen [a,b], Liang Wang [a], Shuang Rong [a], Yuyuan Duan [a], Huizhu Wang [a,*]

[a] College of Chemistry and Pharmaceutical Engineering, Jilin Institute of Chemical Technology, Jilin, Jilin 132022, China
[b] Graduate school, Jilin Institute of Chemical Technology, Jilin, Jilin 132022, China

ARTICLE INFO

*Keywords:*
*Rosa laevigata* Michx.
Polysaccharides
In vitro hypoglycemic activity

ABSTRACT

This study aimed to optimize the extraction process of polysaccharides from *Rosa laevigata* Michx. (RLMP) using an ultrasound-microwave-assisted method and investigate its in vitro hypoglycemic activity. Key factors affecting RLMP yield were identified using a Plackett–Burman design, followed by a Box–Behnken design and response–surface methodology, to determine the optimal extraction conditions. RLMP was purified using DEAE-52 cellulose, yielding two homogeneous fractions: RLMP-1 and RLMP-2. Monosaccharide composition was analyzed by gas chromatography, and structural characterization of RLMP, RLMP-1, and RLMP-2 was performed using FT-IR, SEM, and TEM. Methylation analysis and NMR were used to elucidate the sugar-chain structure of RLMP-1. In vitro hypoglycemic activity analysis showed that RLMP improved the glucose consumption and glycogen synthesis and enhanced the activities of pyruvate kinase and hexokinase in IR-HepG2 cells. Moreover, RLMP significantly increased the activities of antioxidant enzymes, such as CAT, SOD, and GSH-Px and decreased those of ROS and MDA. Western blotting analysis confirmed that RLMP enhances glucose and lipid metabolism and reduces oxidative stress by activating the PI3K/Akt/GLUT-4 signaling pathway, thereby exerting its hypoglycemic effect. These findings suggest that RLMP is a promising candidate for developing novel antioxidant agents or hypoglycemic drugs.

## 1. Introduction

Diabetes mellitus (DM), a systemic chronic metabolic disease, is a significant global health concern, affecting approximately 500 million patients worldwide, and this number is expected to increase to 700 million by 2045 [1,2]. DM can be classified as type 1 DM (T1DM), type 2 DM (T2DM), and gestational DM, among others based on their causes. Among these, T2DM accounts for over 90 % of diabetes cases and is characterized by postprandial hyperglycemia due to insulin secretion deficiency and insulin resistance (IR). Hyperglycemia increases oxidative stress and the production of reactive oxygen species (ROS). This activates the redox-sensitive signaling pathway and blocks the insulin signaling pathway, leading to IR and elevated blood glucose (Glc) levels. Hyperglycemia and oxidative stress interact both causally and through their respective effects on each other [3]. Improving oxidative stress and reducing IR are key strategies in the clinical treatment of diabetes.

Polysaccharides from different natural resources exhibit good antidiabetic activity [4–6]. Upon administration, polysaccharides can reduce blood Glc levels by scavenging free radicals or increasing the activity of antioxidant enzymes, thus inhibiting lipid peroxidation and alleviating cell damage caused by free radicals. Natural polysaccharides with strong antioxidant effects are potential hypoglycemic drugs because of their low toxicity and lack of side effects [7,8].

Belonging to the Rosaceae family, *Rosa laevigata* Michx. (RLM) is a

*Abbreviations:* Fuc, fucose; Fru, fructose; Rib, ribose; GalUA, galacturonic acid; GlcUA, glucuronic acid; GalN, galactosamine hydrochloride; GlcN, glucosamine hydrochloride; GlcNAc, *N*-acetyl-D-glucosamine; GulUA, guluronic acid; ManUA, mannuronic acid; GC, gas chromatography; FT-IR, Fourier transform infrared spectroscopy; SEM, scanning electron microscopy; TEM, transmission electron microscopy; NMR, nuclear magnetic resonance; MDA, malondialdehyde; SOD, superoxide dismutase; CAT, catalase; GSH-Px, reduced glutathione; ROS, reactive oxygen species; IC, ion chromatography; UV, ultraviolet; RIPA, radio immunoprecipitation assay; BCA, disodium bicinchoninate; SDS-PAGE, sodium dodecyl sulfate–polyacrylamide gel electrophoresis; PVDF, polyvinylidene difluoride; TBST, aminomethane hydrochloride; DCFH-DA, dichlorodihydrofluorescein diacetate; CKK-8, cell counting kit-8.

* Corresponding author at: Jilin Institute of Chemical Technology, Chengde Street 45, Jilin 132022, China.
*E-mail address:* whz@jlict.edu.cn (H. Wang).

https://doi.org/10.1016/j.ijbiomac.2024.135116
Received 19 February 2024; Received in revised form 22 August 2024; Accepted 26 August 2024
Available online 28 August 2024

typical traditional medicinal and edible plant widely distributed across southeastern and southwestern China. Its dried and mature fruits have been used to treat polyuria, urinary incontinence, menstrual flow irregularities, uterine prolapse, leucorrhea, and astringency [9,10]. >100 secondary metabolites have been isolated from RLM and identified, including triterpenoids, polysaccharides, flavonoids, organic acids, and tannins. Among these metabolites, polysaccharides from *Rosa laevigata* Michx. (RLMP) are the main active components, and 2020 Chinese Pharmacopoeia stipulates that the RLMP must exceed 25 %. RLMP has several biological activities, including antioxidative, hypolipidemic, and antitumor properties [11–14]. However, further studies are required to investigate whether RLMP exerts hypoglycemic activity and elucidate the underlying potential mechanisms.

Traditional Chinese medicine (TCM) products exhibit remarkable diversity and complexity, necessitating a comprehensive understanding of their constituents. Polysaccharides, a crucial class of compounds in TCM, have varying physicochemical properties and structural characteristics depending on the extraction processes used [15]. The physicochemical and structural properties of polysaccharides are closely associated with their biological activity and functional properties [16,17]. Therefore, selecting an appropriate polysaccharide extraction process is important for studying biological activities. Compared to conventional extraction methods, which are characterized by longer extraction time and lower extraction efficiency, ultrasonic microwave-assisted extraction (UMAE), a technology that utilizes the advantages of ultrasonic vibration for mass transfer and microwave radiation for rapid internal heating to optimize the rate and efficiency of extraction, has been successfully applied to extract natural polysaccharides [18,19]. The extraction efficiency of UMAE is extremely high, approximately 6 times higher than that of hot water extraction [20]. In addition, UMAE improved the antioxidant activity of polysaccharides by modifying their structure [21]. Currently, an industrialized UMAE device called “ultrasonic-microwave synergistic extractor” is commercially available, which allows the application of UMAE in industrial scale.

In this study, UMAE was used to obtain RLMP and the extraction process parameters were optimized. Two homogeneous polysaccharides were obtained by isolation and purification. Structural characterization was performed using FT-IR, monosaccharide composition analysis, methylation analysis, NMR analysis, SEM, and TEM. Furthenmore, hypoglycemic activities and mechanisms of RLMP were evaluated. The findings of this study provide a theoretical foundation for the development of RLMP as functional food ingredients with hypoglycemic effect.

## 2. Materials and methods

### 2.1. Materials and reagents

Dried fruits of RLM were purchased from local drug stores in Changchun, Jilin, China. D-mannose (Man), L-rhamnose (Rha), D-glucose (Glc), D-galactose (Gal), D-xylose (Xyl), and L-arabinose (Ara) were purchased from the National Institutes for Food and Drug Control (Beijing, China). *p*-nitrophenyl-β-D-galactopyranoside (PNPG) was procured from Sigma Chemical Co. (MO, USA). DEAE-cellulose and trifluoroacetic acid (TFA) were purchased from Hefei Bomei Biotechnology Co., Ltd. (Hefei, China). Cyclohexane−1,2,3,4,5,6-hexol (MYO) was purchased from Aladdin Biochemical Polytron Technologies, Inc. (Shanghai, China). α-glucosidase was obtained from JinSui Biotechnology Co., Ltd. (Shanghai, China). Minimum essential medium (MEM), fetal bovine serum (FBS), penicillin–streptomycin, and phosphate-buffered saline (PBS) were purchased from Gibco Life Technologies (Grand Island, NY, USA). Kits for glucose tests and hexokinase (HK), pyruvate kinase (PK), catalase (CAT), superoxide dismutase (SOD), reduced glutathione (GSH), and malondialdehyde (MDA) assays were purchased from Shengyang Wanlei Bioengineering Institute (Shengyang, China). Antibodies against PI3K, phosphorylated PI3K (p-PI3K), Akt, phosphorylated Akt (p-Akt), IRS-1, phosphorylated (p-IRS-1) β-actin, and their corresponding secondary antibodies were obtained from Cell Signaling Technology (MA, USA). All additional chemical reagents used in this study were of analytical grade and purchased locally. Double-distilled water was used in all experiments.

### 2.2. Ultrasound-microwave assisted extraction

RLM was dried in an oven at 100 °C for 4 h, ground to powder using a pulverizer, and filtered through a 40-mesh sieve. For RLMP extraction, 50 g of the powdered sample was mixed with 200 mL of 95 % ethanol (*v*/v) and shaken for 6–10 h to remove fat and small molecules. Following filtration, the obtained filter cake was subjected to extraction on an ultrasound-microwave combined extractor (XH-300B, Xianghu, China) under the following conditions: liquid–solid ratio, 8:1 (mL/g); immersion time, 4 h; microwave temperature, 60 °C; microwave power, 400 W; ultrasonic power, 500 W; ultrasonic time, 20 min; and microwave time, 5 min. After extraction, the supernatants were combined and concentrated to an indicated volume. The mixture was precipitated using 80 % (*v*/v) ethanol at 4 °C for 12 h. Crude polysaccharides were collected by centrifugation at 5000 rpm for 15 min. Polysaccharide content was determined using the phenol-sulfuric method [22]. RLMP yield (*Y*) was calculated as follows:

$$Y(\%) = \frac{polysaccharide\ content\ (g)}{weight\ of\ extract\ (g)} \quad (1)$$

### 2.3. Screening design

PBD was used to identify the main factors affecting RLMP yield. It compares the differences between two levels of each factor and the entire system [23,24]. This study aimed to evaluate the effects of liquid–solid ratio ($X_1$), microwave temperature ($X_2$), microwave power ($X_3$), ultrasonic power ($X_4$), ultrasonic time ($X_5$), microwave time ($X_6$), immersion time ($X_7$), and particle size ($X_8$) on the system. These parameters were varied using a two-level PBD, and the factors and levels tested using Plackett–Burman design are summarized in Table S1. A matrix was established for the eight parameters with 16 group experiments (Table 1).

The effects of different factors on RLMP yield were determined using the first-order model, as described in Eq. (2) below:

$$Y = \beta_0 + E_{x1}x_1 + E_{x2}x_2 + \cdots E_{xi}x_i \quad (2)$$

where $Y$ is the predicted response, $\beta_0$ is the model intercept, and $X_i$ is the level of the $i$th independent variable.

The effect of each argument on the response value was calculated as follows:

$$E_{xi} = \frac{\sum M_{i+} - \sum M_{i-}}{N} \quad (3)$$

where $E_{xi}$ is the influence level for each independent variable, $M_{i+}$ is the

**Table 1**
Plackett–Burman experimental design.

| No. | $X_1$ | $X_2$ | $X_3$ | $X_4$ | $X_5$ | $X_6$ | $X_7$ | $X_8$ | $Y$(%) |
|---|---|---|---|---|---|---|---|---|---|
| 1 | 30 | 60 | 1000 | 1500 | 20 | 20 | 4 | 40 | 25.49 |
| 2 | 8 | 60 | 400 | 1500 | 50 | 20 | 4 | 100 | 27.56 |
| 3 | 8 | 90 | 1000 | 500 | 50 | 5 | 4 | 40 | 26.31 |
| 4 | 8 | 60 | 1000 | 1500 | 50 | 5 | 12 | 100 | 28.3 |
| 5 | 30 | 90 | 1000 | 500 | 50 | 20 | 4 | 100 | 28.16 |
| 6 | 8 | 90 | 1000 | 1500 | 20 | 20 | 12 | 40 | 27.50 |
| 7 | 30 | 60 | 1000 | 500 | 20 | 5 | 12 | 100 | 26.19 |
| 8 | 8 | 60 | 400 | 500 | 20 | 5 | 4 | 40 | 22.58 |
| 9 | 8 | 90 | 400 | 500 | 20 | 20 | 12 | 100 | 25.28 |
| 10 | 30 | 90 | 400 | 1500 | 20 | 5 | 4 | 100 | 27.77 |
| 11 | 30 | 60 | 400 | 500 | 50 | 20 | 12 | 40 | 26.36 |
| 12 | 30 | 90 | 400 | 1500 | 50 | 5 | 12 | 40 | 30.70 |

maximum predictive response value, $M_i$. is the minimum predictive response, and $N$ is the number of trials.

### 2.4. Optimization design

RSM was used to optimize the process parameters. Experimental runs and data processing were performed in the Design Expert (V8.0.6.1) software. The combined effects of ultrasonic time (30, 40, and 50 min), microwave temperature (70, 80, and 90 °C), ultrasonic power (600, 800, and 1000 W), liquid–solid ratio (15:1, 20:1, and 25:1 mL/g), and immersion time (6, 8, and 10 h) on the final RLMP yield were investigated using the BBD. The selected factors and levels are summarized in Table S2. The complete experimental design comprised 40 experimental points and 6 replicates at the center point to estimate a pure error sum of squares [25,26]. All experiments were conducted following the BBD matrix (Table 2).

A quadratic polynomial model was established using multiple regression of the experimental data as follows:

$$Y = \beta_0 + \sum_{i=1}^{5} \beta_{ki} X_i + \sum_{i<j=2}^{5} \beta_{kij} X_i X_j + \sum_{i=1}^{5} \beta_{kii} X_i^2 \quad (4)$$

where $Y$ is the response value; $\beta_0$ is the regression coefficient for a constant; $\beta_i$, $\beta_{ii}$, and $\beta_{ij}$ are the linear, quadratic, and interaction terms, respectively, of the $A$, $B$, $C$, $D$, and $E$ $_s$ factors on the response; and $X_i$ and $X_j$ are coded-independent variables.

**Table 2**
Box–Behnken experimental design.

| No. | A | B | C | D | E | Y (%) |
|---|---|---|---|---|---|---|
| 1 | 0(40) | 0(80) | 0(800) | −1(15) | −1(6) | 25.80 |
| 2 | −1(30) | 0(80) | 0(800) | 0(20) | −1(6) | 26.15 |
| 3 | 0(40) | 0(80) | 0(800) | 0(20) | 0(8) | 29.73 |
| 4 | 0(40) | −1(70) | 1(1000) | 0(20) | 0(8) | 28.40 |
| 5 | −1(30) | 0(80) | −1(600) | 0(20) | 0(8) | 27.66 |
| 6 | −1(30) | 0(80) | 0(800) | −1(15) | 0(8) | 28.21 |
| 7 | 0(40) | 1(90) | 0(800) | −1(15) | 0(8) | 29.15 |
| 8 | 0(40) | −1(70) | 0(800) | 0(20) | −1(6) | 25.12 |
| 9 | 0(40) | 1(90) | 1(1000) | 0(20) | 0(8) | 29.07 |
| 10 | 0(40) | 0(80) | 1(1000) | 1(25) | 0(8) | 27.78 |
| 11 | 0(40) | −1(70) | 0(800) | 0(20) | 1(10) | 28.14 |
| 12 | −1(30) | 0(80) | 0(800) | 0(20) | 1(10) | 27.55 |
| 13 | 0(40) | 0(80) | −1(600) | 0(15) | 0(8) | 25.57 |
| 14 | 0(40) | 0(80) | 0(800) | 0(20) | 0(8) | 31.11 |
| 15 | −1(30) | 0(80) | 0(800) | 1(25) | 0(8) | 27.61 |
| 16 | 1(50) | 0(80) | 0(800) | 0(15) | 0(8) | 27.93 |
| 17 | 1(50) | −1(70) | 0(800) | 0(20) | 0(8) | 28.22 |
| 18 | 1(50) | 0(80) | 0(800) | 0(20) | −1(6) | 27.56 |
| 19 | 0(40) | 0(80) | 0(800) | 0(20) | 0(8) | 30.23 |
| 20 | −1(30) | 1(90) | 0(800) | 0(20) | 0(8) | 27.15 |
| 21 | 1(50) | 0(80) | 1(1000) | 0(20) | 0(8) | 29.11 |
| 22 | 0(40) | 1(90) | 0(800) | 1(25) | 0(8) | 29.07 |
| 23 | 0(40) | 0(80) | −1(600) | 1(25) | 0(8) | 27.14 |
| 24 | 0(40) | 1(90) | −1(600) | 0(20) | 0(8) | 28.33 |
| 25 | 0(40) | 0(80) | 0(800) | 0(20) | 0(8) | 29.57 |
| 26 | 0(40) | 0(80) | 0(800) | −1(15) | 1(10) | 28.77 |
| 27 | 0(40) | 0(80) | −1(600) | 0(20) | 1(10) | 26.96 |
| 28 | 0(40) | 0(80) | 0(800) | 0(20) | 0(8) | 29.97 |
| 29 | −1(30) | 0(80) | 1(1000) | 0(20) | 0(8) | 28.14 |
| 30 | 0(40) | −1(70) | 0(800) | 1(25) | 0(8) | 27.46 |
| 31 | 0(40) | −1(70) | 0(800) | −1(15) | 0(8) | 26.81 |
| 32 | 0(40) | 0(80) | −1(600) | 0(20) | −1(6) | 26.32 |
| 33 | −1(30) | −1(70) | 0(800) | 0(20) | 0(8) | 27.77 |
| 34 | 0(40) | 0(80) | 1(1000) | 0(20) | −1(6) | 30.11 |
| 35 | 1(50) | 0(80) | −1(600) | 0(20) | 0(8) | 29.65 |
| 36 | 1(50) | 0(80) | 0(800) | 0(20) | 1(10) | 28.81 |
| 37 | 0(40) | 0(80) | 0(800) | 0(20) | 0(8) | 30.55 |
| 38 | 0(40) | 1(90) | 0(800) | 0(20) | 1(10) | 27.12 |
| 39 | 0(40) | 0(80) | 1(1000) | −1(15) | 0(8) | 27.98 |
| 40 | 0(40) | 0(80) | 0(800) | 1(25) | 1(10) | 26.87 |
| 41 | 0(40) | 1(90) | 0(800) | 0(20) | −1(6) | 29.25 |
| 42 | 0(40) | −1(70) | −1(600) | 0(20) | 0(8) | 27.74 |
| 43 | 0(40) | 0(80) | 1(1000) | 0(20) | 1(10) | 29.04 |
| 44 | 1(50) | 1(90) | 0(800) | 0(20) | 0(8) | 28.45 |
| 45 | 0(40) | 0(80) | 0(800) | 1(25) | −1(6) | 27.78 |
| 46 | 1(50) | 0(80) | 0(800) | 1(25) | 0(8) | 29.91 |

### 2.5. Comparison of extraction methods

Heat-reflux extraction (HRE), ultrasonic-assisted extraction (UAE), and microwave-assisted extraction (MAE) of polysaccharides from RLM were performed at the following parameters: immersion time of 8 h, and liquid–solid ratio of 20:1. HRE was performed at 100 °C with an extraction time of 4 h. UAE was performed for 45 min at 850 W. MAE was performed for an extraction time of 45 min at a microwave temperature of 85 °C. The RLMP yield under the three extraction methods was measured using the phenol-sulfuric acid method.

### 2.6. Polysaccharide purification

Proteins in RLMP were removed using the Sevage method. Subsequently, the polysaccharides were dissolved in deionized water and loaded onto a DEAE-52 cellulose column (3 × 30 cm) for elution. At the indicated time points, water, 0.1 mol/L NaCl, and 0.3 mol/L NaCl were used as elution solvents at a flow rate of 1.5 mL/min. The eluate was collected using an automatic collector, and the polysaccharide content was determined using the phenol-sulfuric method. The same components were combined, concentrated, and packed into a dialysis bag to remove NaCl. Finally, two fractions were obtained, namely RLMP-1 and RLMP-2.

### 2.7. Monosaccharide composition

Polysaccharide derivatization was carried out using the literature method with some modifications [27]. A 10 mg polysaccharide sample was hydrolyzed with 4 mol/L trifluoroacetic acid. After hydrolysis, the supernatant was purified with methanol to remove excess acid. The residue was dissolved in water and transferred to a volumetric flask. Reduction was performed with pyridine and hydroxylamine hydrochloride at 100 °C. Acetylation followed by adding acetic anhydride and incubating at 100 °C. Rha, Ara, Xyl, Man, Glc, and Gal standards were derivatized using the same procedure.

Monosaccharide composition analysis of RLMP was conducted using a gas chromatograph (7820 A, Agilent Technologies, Santa Clara, CA, USA), equipped with a 7693 A automatic sampler and an Agilent HP-5 capillary column (30 m × 0.32 mm, 0.25 μm). Experimental parameters were as follows: carrier gas, nitrogen; flow rate, 1.5 mL/min; auxiliary gases, hydrogen and air at rates of 30 mL/min and 300 mL/min, respectively; detector temperature, 280 °C; sample injector temperature, 210 °C; injection volume, 0.2 μL; and split flow ratio, 10:1. The temperature of the chromatographic column was initially set at 90 °C and maintained for 2 min. It was increased to 160 °C at a rate of 7 °C/min and maintained for 3 min. It was then and raised to 190 °C at a rate of 3 °C/min and maintained for 5 min. Eventually, the temperature was increased to 200 °C at a rate of 5 °C/min and maintained for 5 min. The internal standard was cyclohexane-1,2,3,4,5,6-hexol.

### 2.8. Characterization of polysaccharides

#### 2.8.1. UV spectroscopy

RLMP-1 and RLMP-2 was dissolved in distilled water to form a solution of 0.6 mg/mL. The UV absorption spectrum of the solution was recorded in the wavelength range of 200–400 nm using a UV–vis spectrophotometer (TU-1950, Beijing Puxi General Instrument Co., Ltd., Beijing, China). The protein content was analyzed using the Coomassie Brilliant Blue method [28], with bovine serum albumin (BSA) as the standard.

#### 2.8.2. Molecular weight distribution

The homogeneity and molecular weight distributions of RLMP-1 and RLMP-2 were examined by high-performance gel permeation chromatography (HPGPC) using a Waters 1515 HPLC instrument equipped with a Waters Ultrahydrogel column (250 A, 6 μm, 7.8 × 300 mm) and a refractive index detector [29,30]. A polysaccharide sample (30 mg) was weighed and placed in a 100-mL volumetric flask. Deionized water was added to the flask up to the marked line, and the solution was mixed thoroughly and filtered through a 0.45-μm microporous membrane before injection. The chromatographic system comprised a mobile phase of 0.1 M sodium nitrate aqueous solution, with column and detector temperatures maintained at 40 °C and a flow rate of 1.0 mL/min. Molecular weights in the range of 500 and 10,000 Da were detected. Pullulan standards were used to obtain a calibration curve, and the molecular weights of the polysaccharides were calculated based on the standard curve.

#### 2.8.3. FT-IR analysis

RLMP, RLMP-1, and PLMR-2 were subjected to FT-IR analysis using a Nicolet 6700 FT-IR spectrometer (Thermo Fisher Scientific, USA). Samples were ground with KBr powder and pressed into 1-mm pellets for measurement. Results were recorded in the range of 4000–400 $cm^{-1}$ at a resolution of 8 $cm^{-1}$.

#### 2.8.4. Methylation analysis

Methylation analysis was conducted to determine the types of glycosyl linkages present in the RLMP-1 sample [31]. RLMP-1 was sequentially methylated, hydrolyzed, reduced, and acetylated to obtain partially methylated alcohol acetates (PMAAs) of RLMP-1, which were further analyzed by GC/MS.

#### 2.8.5. NMR

RLMP-1 was subjected to deuterium exchange in $D_2O$ thrice. The sample (50 mg) was dissolved in $D_2O$ (0.5 mL). $^1D$ NMR was conducted with $^1H$ NMR, and $^{13}C$ NMR and 2D NMR (COSY, HSQC, HMBC, and NOESY) data analyses were performed [32] on an NMR spectrometer (Avance III HD 600 MHz, Brucker, Germany).

#### 2.8.6. SEM and TEM

The morphological and surface characteristics of RLMP, RLMP-1, and PLMR-2 were observed and recorded using SEM. A drop of polysaccharide sample solution (5 μg/mL) was added to the mica, and gold was sprayed after drying. An S-4800 field emission scanning electron microscope (S-4800, Hitachi, Japan) was used for observation and image collection.

The microscopic structures of the polysaccharides were observed by TEM [33]. Samples were dissolved in distilled water, ultrasonicated for 20 min, and immediately dropped onto copper mesh for testing. A high-resolution field emission transmission electron microscope (FEI Talos F200S 200 kV, Thermo Scientific, US) was used for observation and image collection.

**Table 3**
Analysis of variance for the Plackett-Burman test.

| Source | df | Adj SS | Adj MS | F | P | Inference |
|---|---|---|---|---|---|---|
| Model | 8 | 42.9084 | 5.3636 | 15.77 | 0.022 | * |
| Linear | 8 | 42.9084 | 5.3636 | 15.77 | 0.022 | * |
| $X_1$ | 1 | 4.2483 | 4.2483 | 12.49 | 0.039 | * |
| $X_2$ | 1 | 7.1148 | 7.1148 | 20.92 | 0.020 | * |
| $X_3$ | 1 | 0.2408 | 0.2408 | 0.71 | 0.462 | – |
| $X_4$ | 1 | 12.8961 | 12.8961 | 37.92 | 0.009 | ** |
| $X_5$ | 1 | 13.188 | 13.188 | 38.77 | 0.008 | ** |
| $X_6$ | 1 | 0.1875 | 0.1875 | 0.55 | 0.512 | – |
| $X_7$ | 1 | 3.4776 | 3.4776 | 10.22 | 0.049 | * |
| $X_8$ | 1 | 1.5552 | 1.5552 | 4.57 | 0.122 | – |
| Residual | 3 | 1.0204 | 0.3401 | | | |
| Cortotal | 11 | 43.9288 | | | | |

–: means not significant.
** Means highly significant ($P < 0.01$).
* Means significant ($P < 0.05$).

**Table 4**
ANOVA of the response surface quadratic model.

| Source | Sum of squares | DF | Mean square | F | p | |
|---|---|---|---|---|---|---|
| Model | 64.52 | 20 | 3.23 | 4.77 | 0.000 2 | ** |
| A | 5.52 | 1 | 5.52 | 8.16 | 0.008 5 | ** |
| B | 3.93 | 1 | 3.93 | 5.81 | 0.023 6 | * |
| C | 6.58 | 1 | 6.58 | 9.73 | 0.004 5 | ** |
| D | 0.72 | 1 | 0.72 | 1.07 | 0.311 3 | – |
| E | 1.67 | 1 | 1.67 | 2.47 | 0.128 7 | – |
| AB | 0.18 | 1 | 0.18 | 0.27 | 0.6099 | – |
| AC | 0.26 | 1 | 0.26 | 0.38 | 0.5408 | – |
| AD | 1.66 | 1 | 1.66 | 2.46 | 0.1294 | – |
| AE | 5.625E-003 | 1 | 5.625E-003 | 8.315E-003 | 0.9281 | – |
| BC | 1.600E-003 | 1 | 1.600E-003 | 2.365E-003 | 0.9616 | – |
| BD | 0.13 | 1 | 0.13 | 0.20 | 0.6610 | – |
| BE | 6.63 | 1 | 6.63 | 9.80 | 0.0044 | ** |
| CD | 0.78 | 1 | 0.78 | 1.16 | 0.2922 | – |
| CE | 0.73 | 1 | 0.73 | 1.08 | 0.3085 | – |
| DE | 3.76 | 1 | 3.76 | 5.56 | 0.0265 | * |
| $A^2$ | 6.30 | 1 | 6.30 | 9.31 | 0.0053 | ** |
| $B^2$ | 9.97 | 1 | 9.97 | 14.74 | 0.000 7 | ** |
| $C^2$ | 7.43 | 1 | 7.43 | 10.99 | 0.0028 | ** |
| $D^2$ | 15.97 | 1 | 15.97 | 23.61 | <0.000 1 | ** |
| $E^2$ | 21.25 | 1 | 21.25 | 31.41 | <0.000 1 | ** |
| Residual | 16.91 | 25 | 0.68 | | | |
| Lack of fit | 15.29 | 20 | 0.76 | 2.36 | 0.1737 | – |
| Pure Error | 1.62 | 5 | 0.32 | | | |
| Correct Total | 81.43 | 45 | | | | |
| R-Squared | 0.7923 | | | | | |
| Adjusted R-square | 0.6262 | | | | | |

–: means not significant.
** Means highly significant ($P < 0.01$).
* Means significant ($P < 0.05$).

### 2.9. Assessment of hypoglycemic activity

#### 2.9.1. α-Glucosidase inhibitory activity

The α-glucosidase inhibitory activity of RLMP was measured using PNPG as the substrate and acarbose as the positive control [34]. Various volumes of the sample, α-glucosidase solution (40 μL, 4200 U/mL), and phosphate buffer (pH 6.8) were added into 96-well plates, and the final volume of each reaction system was made to 260 μL. After pre-incubation at 37 °C for 20 min, PNPG (30 μL, 20 mmol/L) was added and incubated for another 20 min. The reaction was stopped with sodium carbonate, and absorbance was measured at 405 nm. All samples were analyzed in a triplicate. The inhibitory rate was calculated using Eq. (5). The half-maximal inhibitory concentration ($IC_{50}$) values were calculated using GraphPad Prism (version 9.5.1).

$$Inhibitory\ rate = \left(1 - \frac{A_c - A_d}{A_a - A_b}\right) \times 100\% \quad (5)$$

where $A_a$ is the absorbance of buffer solution, enzyme liquid, and substrate; $A_b$ is the absorbance of buffer solution; $A_c$ is the absorbance of sample solution, enzyme liquid, and substrate, and $A_d$ is the absorbance of sample and buffer solutions.

#### 2.9.2. Cytotoxicity assay

HepG2 cells were grown in MEM containing 10 % FBS in an incubator at 37 °C with 5 % $CO_2$. Cells in the logarithmic growth phase were selected and digested, and the cell suspension was aspirated and added

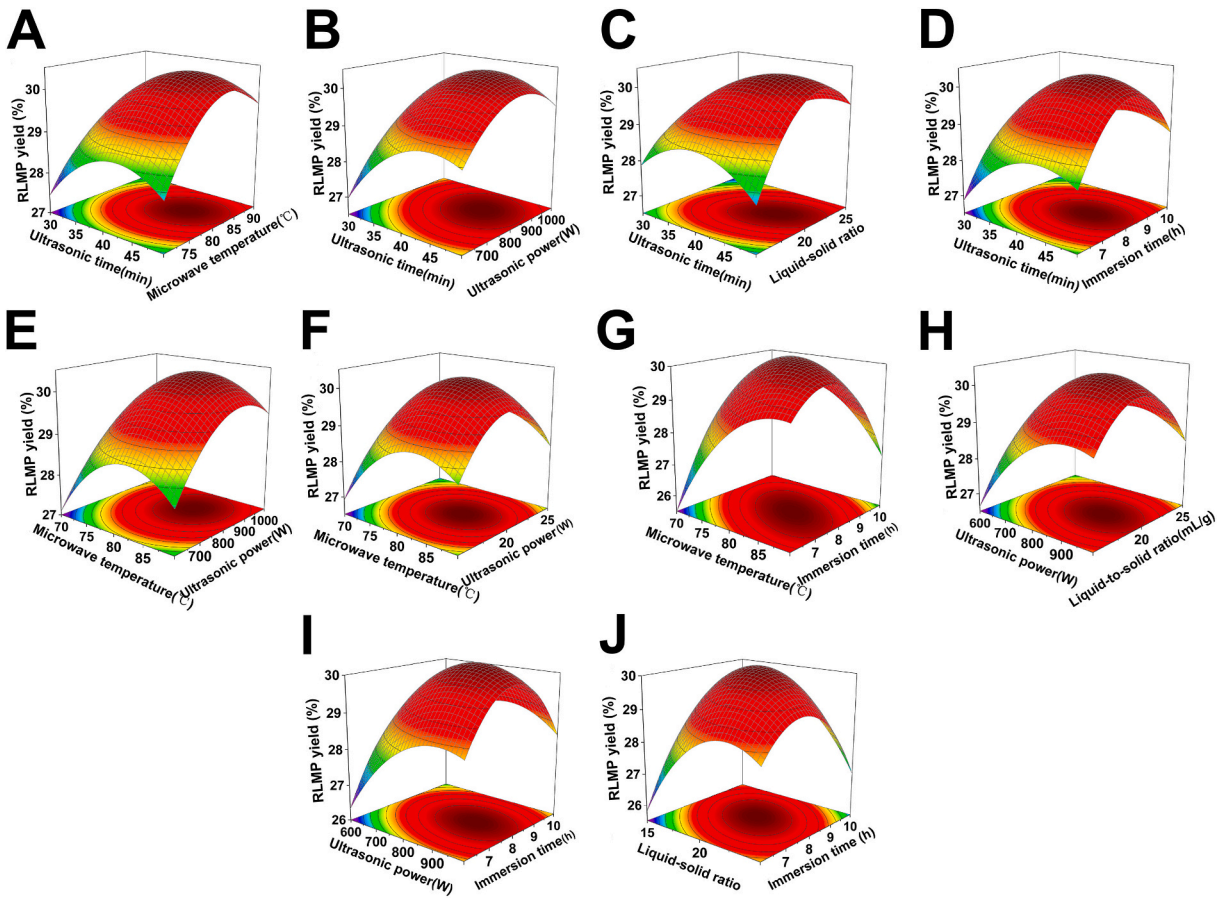


**Fig. 1.** 3D response surface plots showing the effect of two variables on RLMP yield while the remaining two kept at coded zero level. Ultrasonic time and microwave temperature (A), Ultrasonic time and power (B), Ultrasonic time and liquid-solid ratio (C), Ultrasonic time and immersion time (D), Microwave temperature and ultrasonic power (E), Microwave temperature and liquid-solid ratio (F), Microwave temperature and immersion time (G), Ultrasonic power and liquid-solid ratio (H), Ultrasonic power and immersion time (I), liquid-solid ratio and immersion time (J).

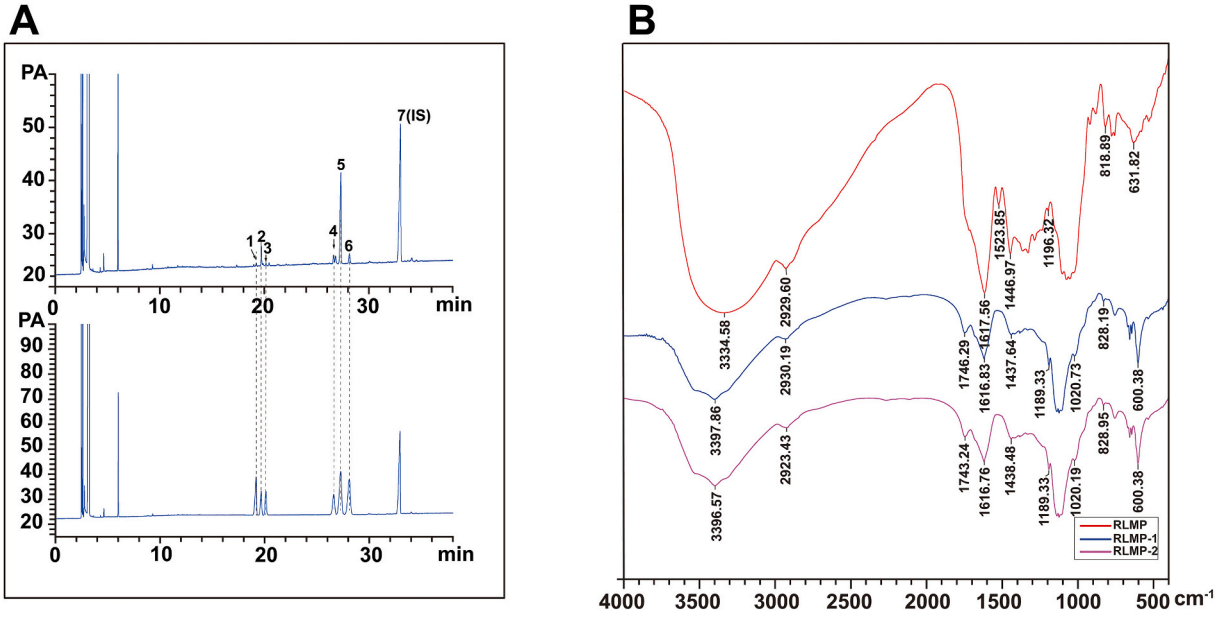


**Fig. 2.** GC chromatogram of RLMP (A) (1-Rha, 2-Ara, 3-Xyl, 4-Man, 5-D-Glu, and 6-Gal) and the standard substance mixture (B), FT-IR spectra of RLMP, RLMP-1 and RLMP-2 (C).

to PBS. Trypan blue dye was added, and the mixture was kept at 25 °C. Cells were counted using a fluorescence microscope. After dilution based on the counting results, cells were evenly inoculated into 96-well plates and placed in an incubator. After 24 h, 100 μL of polysaccharide solutions at 0.1, 0.3, 0.6, 0.8, and 1.0 mg/mL were added to the wells, and the plates were incubated for another 24 h. Then, cells were treated according to the CKK-8 kit's manufacturer's instructions. The wells without polysaccharide solution served as blank controls. Cell survival rate was calculated based on the absorbance value of each well at 490 nm.

#### 2.9.3. Glc consumption assay

A glucose consumption assay was performed using insulin-resistant HepG2 (IR-HepG2) cells, as previously described with slight modifications [35]. Experiments were conducted in normal, model, positive control, and sample groups. Cells were seeded in MEM containing insulin (0.5 μM) for 24 h. The medium was replaced, and cells were treated with three different concentrations of RLMP: low (0.1 mg/mL), medium (0.3 mg/mL), or high (0.6 mg/mL). Cells were continuously cultured for 24 h. Then, the culture medium was collected and centrifuged, and the Glc content in the supernatant was determined.

#### 2.9.4. Glycogen content and HK and PK activities

HepG2 cells were cultured into six-well plates at a density of $5 \times 10^4$ cells/mL and incubated for 24 h. Then, IR-HepG2 cells were established according to the above description. Cells were collected and treated with cell lysis buffer at 4 °C for 10 min. The glycogen content of cell lysates was quantified using the Glycogen Content Assay Kit and BCA Protein Concentration Assay Kit. HK and PK activities were tested using their respective kits.

### 2.10. In vitro antioxidant activity

#### 2.10.1. ROS levels

The ROS inhibitory activity of RLMP was assessed following Cao et al.'s method [36]. After treatment with different concentrations of RLMP (0.1, 0.3, and 0.6 mg/mL), the cells were rinsed with PBS and incubated with DCFH-DA (10 μM) for 20 min in the dark at 37 °C. They were then rinsed twice with PBS and analyzed using a fluorescence spectrophotometer with excitation and emission wavelengths of 485 and 535 nm, respectively. The positive control group was treated with metformin.

#### 2.10.2. CAT, SOD, and GSH-Px activities and MDA content

HepG2 cells were inoculated into six-well plates and grown in medium containing RLMP for 24 h. Cells were lysed and centrifuged, and supernatants were collected and analyzed to determine CAT, SOD, and GSH-Px activities and MDA content using their corresponding kits.

### 2.11. Western blotting analysis

Western blotting analysis was conducted as previously described [37]. HepG2 cells were grown and grouped as follows: normal, model, positive (MET media), and with different concentrations of RLMP dissolved in MEM for 24 h. Total proteins were extracted using RIPA buffer, centrifuged, and quantified using a BCA kit. Thereafter, 40 μg of proteins were resolved using 10 % SDS-PAGE and transferred onto PVDF membranes blocked with 5 % skim milk in TBST for 1 h. Subsequently, the membranes were incubated with p-PI3K (1:500 dilution), PI3K (1:500), p-Akt (1:500), Akt (1:1000), p-IRS − 1 (1:500), IRS − 1 (1:300), GLUT4 (1:500), and β-actin (1:1000) antibodies overnight at 4 °C. The blots were washed with TBST buffer thrice and inoculated with goat anti-rabbit IgG (1:5000) secondary antibody for 45 min at 25 °C. Protein bands were visualized by electrochemiluminescence and analyzed using the Gel-Pro-Analyzer software.

### 2.12. Statistical analysis

All experimental data are presented as the mean ± SD and were analyzed in GraphPad Prism (GraphPad Software, Boston, USA, version 9.5.1). Data were evaluated for significance using one-way analysis of variance (ANOVA), followed by Tukey's post-hoc test. Significant differences between groups at different levels were identified as follows: $^*p < 0.05$, $^{**}p < 0.01$, and $^{***}p < 0.001$.

## 3. Results

### 3.1. PBD

As shown in Table 3, The $p$ values for the ultrasonic time ($X_5$), microwave temperature ($X_2$), ultrasonic power ($X_4$), liquid–solid ratio ($X_1$), and immersion time ($X_7$) were <0.05, indicating that the effects of these factors on polysaccharide yield were significant at a 95 % confidence interval. The Pareto plots (Fig. S1) show the relative importance of the corresponding factors ($X_1$ to $X_8$) on polysaccharide yield. The standardized effect value was used to quantify the effect of the factor on the yield, with larger values indicating a greater effect. At a standardization effect >3.182, ultrasonic time, microwave temperature, ultrasonic power, liquid–solid ratio, and immersion time exhibited significant effects on the polysaccharide yield, consistent with the results in Table 3. Therefore, these five factors were selected to further optimize the extraction process.

### 3.2. RSM analysis

The BBD experimental data were analyzed using Design Expert software 8.0.6.1. Relationships between the response value and test variables were established using the second-order polynomial equation shown in Eq. (6), where the response value is denoted by $Y$. ANOVA with the quadratic model is shown in Table 4.

$$Y = -187.6 + 0.4274\,A + 2.255B + 0.06182C + 3.113D + 14.42E + 2.125E{-}03AB - 1.280E{-}04\,AC + 0.01290\,AD - 1.875E{-}03\,AE + 1.000E{-}05\,BC - 3.650E{-}03BD - 0.06438BE - 4.43E{-}04CD - 1.069E{-}03\,CE - 0.097DE - 8.496E{-}03A^2 - 0.01069B^2 - 2.300E{-}05C^2 - 0.05412D^2 - 0.3901E^2 \quad (6)$$

As listed in Table 4, the $p$-value of the model was highly significant ($p < 0.01$), while the $p$-value of the lack of fit was 0.1737, suggesting no significance and verifying the model's validity. The $R^2$ value of 0.7923 and adjusted $R^2$ value of 0.6262 confirmed the model's reliability and its goodness of fit [27]. Notably, the model response value was obtained using significant linear coefficients ($A$, $B$, and $C$), interaction term coefficients ($BE$, $DE$), and quadratic term coefficients ($A^2$, $B^2$, $C^2$, $D^2$, and $E^2$) ($p < 0.05$), and the lack of a significant effect of $D$ and $E$ ($p > 0.05$) demonstrated the lack of effect of these values on the RLMP content. The increasing order of effects of the factors was ultrasonic power ($C$) > ultrasonic time ($A$) > microwave temperature ($B$) > immersion time ($E$) > liquid–solid ratio ($D$).

Three-dimensional (3D) graphs were plotted with the response value ($Y$) on the $Z$-axis against any two factors, with the remaining factors held constant at their center point values (coded value = 0) to visualize the interactions between two independent variables. Fig. 1A–J show the effects of the independent variable interactions on the RLMP yield, with significant factors indicated based on the surface steepness. The optimal conditions for RLMP yield were identified by the circle's center shown in the contours. Optimum conditions were as follows: ultrasonic power, 857.45 W; ultrasonic time, 44.05 min; microwave temperature, 83.38 °C; immersion time, 7.75 h, and liquid–solid ratio, 20.75:1 (mL/g). Considering real-life operating convenience in production, the optimum conditions with a predicted RLMP content of 30.48 % were adjusted as follows: ultrasonic power, 850 W; ultrasonic time, 45 min; microwave temperature, 85 °C; immersion time, 8 h, and liquid–solid ratio, 20:1 (mL/g). Procedural accuracy and stability were verified

**Table 5**
Methylated analysis results for RLMP-1.

| Retention time | Methylated sugar | Mass fragments (*m/z*) | Molar ratio | Type of linkage |
|---|---|---|---|---|
| 10.329 | 2,3,5-$Me_3$-Araf | 45,71,87,101,117,129,145,161 | 0.199 | Araf-(1→ |
| 14.994 | 2,3-$Me_2$-Araf | 45,71,87,99,101,117,129,161,189 | 0.122 | →5)-Araf-(1→ |
| 16.749 | 2,3,4,6-$Me_4$-Glcp | 45,71,87,101,117,129,145,161,205 | 0.174 | Glcp-(1→ |
| 20.809 | 2,3,6-Me3-Manp | 45,87,99,101,113,117,129,131,161,173,233 | 0.076 | →4)-Manp-(1→ |
| 21.168 | 2,3,6-$Me_3$-Glcp | 45,87,99,101,113,117,129,131,161,173,233 | 0.151 | →4)-Glcp-(1→ |
| 21.91 | 2,4,6-$Me_3$-Galp | 45,87,99,101,117,129,161,173,233 | 0.216 | →3)-Galp-(1→ |
| 22.748 | 2,3,4-$Me_3$-Galp | 45,87,99,101,117,129,161,189,233 | 0.054 | →6)-Galp-(1→ |
| 26.367 | 2,3-$Me_2$-Glcp | 45,71,85,87,99,101,117,127,159,161,201,261 | 0.245 | →4,6)-Glcp-(1→ |
| 28.88 | 2,4-$Me_2$-Galp | 45,87,117,129,159,189,233 | 0.084 | →3,6)-Galp-(1→ |

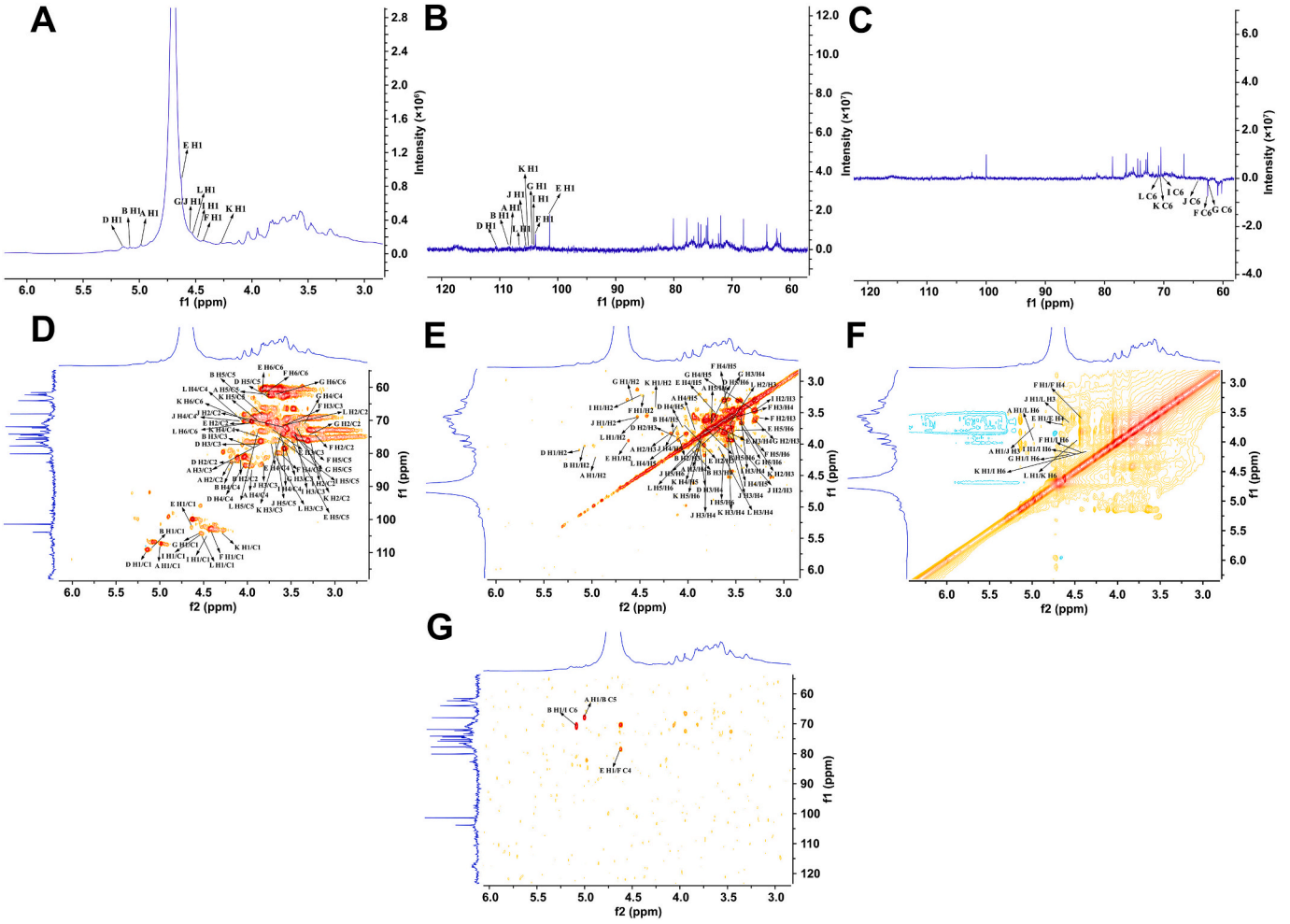


**Fig. 3.** $^{1}$D and $^{2}$D NMR spectra of RLMP-1. $^{1}$H NMR spectrum (A), $^{13}$C NMR spectrum (B), HSQC spectrum (C), DEPT 135 spectrum (D), $^{1}$H—$^{1}$H COSY spectrum (E), NOESY spectrum (F), HMBC spectrum (G).

through three parallel experiments, yielding an average RLMP content of 30.12 %, with a relative error of 1.2 %, indicating the consistency between the actual and predicted values.

### 3.3. Comparison of extraction methods

It can be seen from Fig. S2 that the RLMP yield obtained using UMAE (30.12 %) was significantly higher than yield from UAE (28.45 %), MAE (27.33 %), and HRE (26.13 %). The yield using HRE was significantly lower than those using UAE and MAE ($p < 0.01$). Additionally, the yield using UAE was significantly higher than that using MAE ($p < 0.05$). These results indicate that ultrasonication and microwave treatment enhance RLMP extraction efficiency.

### 3.4. Monosaccharide composition

As shown in Fig. 2A, the six standard monosaccharides were successfully separated within 35 min. The monosaccharide composition of the sample was identified by aligning the retention times and using the standard addition method with those of the standards. The predominant monosaccharides present in RLMP were Rha, Ara, Xyl, Man, D-Glc, and Gal, with a molar ratio of 1.0:20.7:4.3:7.4:65.3:10.8. Among them, Ara, D-Glc, and Gal were the most abundant monosaccharides in RLMP.

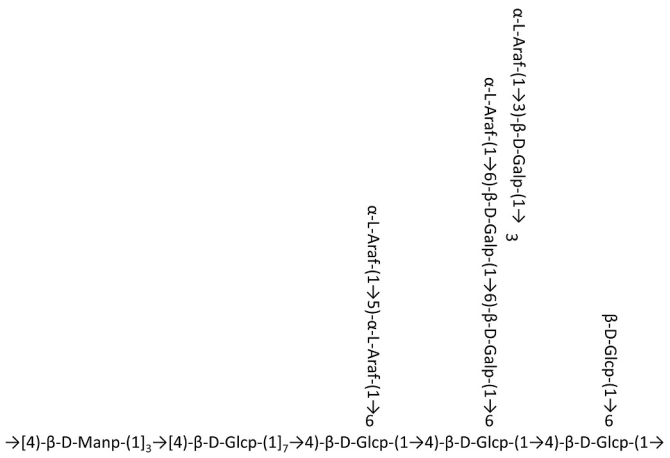


**Fig. 4.** The structure link of RLMP-1.

### 3.5. Characterization of polysaccharides

#### 3.5.1. UV–vis spectra

Fig. S4 shows the UV–visible spectra of RLMP-1 and RLMP-2 in the wavelength range of 200–400 nm. The absorbance at 280 nm confirms the presence of protein in RLMP-1 and RLMP-2, with protein contents of 3.42 % and 4.07 %, respectively. Moreover, the absence of absorbance at 260 nm indicates that nucleic acids are not present in either sample.

#### 3.5.2. Distribution of molecular weights

The homogeneity and molecular weights of the two purified polysaccharides were determined by HPGPC (Fig. S5). The average molecular weights of RLMP-1 and RLMP-2 were 12.3 kDa and 8.3 kDa, respectively, representing low-molecular-weight polysaccharides [13]. The purity of RLMP-1 was calculated using the peak area normalization method, yielding a purity of 82.2 %. This indicates that RLMP-1 is not a single homogeneous polysaccharide. However, comparing the chromatograms of RLMP-1 and RLMP-2, RLMP-1 has a higher degree of homogeneity as a polysaccharide. Further methylation analysis and NMR tests were conducted to gain insights into the structural characteristics of RLMP-1.

#### 3.5.3. FT-IR analysis

Infrared spectroscopy analysis revealed differences in the characteristic peaks of RLMP before and after purification (Fig. 2B). In RLMP, the broad absorption band at 3500–3300 $cm^{-1}$ is attributed to O—H stretching vibrations, whereas the weak absorption peak at 2930 $cm^{-1}$ is attributed to C—H stretching vibrations. The characteristic absorption peak at 1600 $cm^{-1}$ corresponds to C═O stretching vibrations or hydrated hydroxyl groups [38,39]. Additionally, multiple characteristic peaks of pyranose sugars are observed in the fingerprint region of 1000–1200 $cm^{-1}$, which are typically attributed to C-O-C and C-O-H vibrations [40]. The weak absorption peak at 830 $cm^{-1}$ is characteristic of α-glycosidic bonds [41,42]. In RLMP-1 and RLMP-2, the O—H and C—H stretching vibration peaks remain at approximately 3400 $cm^{-1}$ and 2920 $cm^{-1}$, respectively. However, the absorption peaks at 1000–1200 $cm^{-1}$ are simplified, suggesting that some impurities or non-polysaccharide components were removed during separation and purification. Although the main absorption peaks are retained, changes in their intensity and position indicate the effect of the purification process on the polysaccharide structure.

#### 3.5.4. Methylation analysis

Based on the determination of monosaccharide composition of RLMP-1 by ion chromatography (Fig. S6 and Table S3), GC–MS analyses were conducted to determine the types of glycosyl linkages present in RLMP-1, and the results are summarized in Table 5 and illustrated in Fig. S6. RLMP-1 contained (1→)-linked Araf, (1 → 5)-linked Araf, (1→)-linked Glcp, (1 → 4)-linked Manp, (1 → 4)-linked Glcp, (1 → 3)-linked Galp, (1 → 6)-linked Galp, (1 → 4,6)-linked Glcp, and (1 → 3,6)-linked Galp.

#### 3.5.5. NMR analysis

As shown in Fig. 3A, intricate anomeric proton signals spanning from δ3.2 to δ4.0 ppm represent the sugar proton ring, and the primary terminal proton peaks at δ5.15, 5.08, 5.00, 4.64, 4.55, 4.47, 4.45, 4.41, and 4.37 are concentrated in the 4.3–5.5 ppm region, indicating that RLMP-1 is a heteropolysaccharide with multiple glycosidic linkages. The anomeric carbon signal (90.0–110.0 ppm) suggests the presence of both α- and β-configurations in RLMP-1 [16]. Other anomeric signals in the HSQC spectrum of RLMP-1 (Fig. 3C), including that at 5.0/108.77 ppm, 5.08/108.88 ppm, 5.15/110.62 ppm, 4.64/101.49 ppm, 4.41/103.84 ppm, 4.55/104.2 ppm, 4.45/103.83 ppm, 4.55/105.39 ppm, 4.37/104.9 ppm, and 4.47/104.69 ppm, were assigned to α-L-Araf-(1→, →5)-α-L-Araf-(1→, α-L-Araf-(1→, →4)-α-D-Manp-(1→, →4)-β-D-Glcp-(1→, β-D-Glcp-(1→, →4,6)-β-D-Glcp-(1→, →3)-β-D-Galp-(1→, →6)-β-D-Galp-(1→, →3,6)-β-D-Galp-(1→, respectively.

According to the $^{1}H—^{1}H$ COSY spectrum of RLMP-1 (Fig. 3E), the correlation peaks at 5.15/4.13 ppm, 4.13/3.87 ppm, 3.87/4.06 ppm, and 4.06/3.76 ppm are attributed to the H-1/H-2, H-2/H-3, H-3/H-4, and H-4/H-5, respectively, of α-L-Araf-(1→, leading to the assignments of the chemical shifts of the H-2 (4.13 ppm), H-3 (3.87 ppm), H-4 (4.06 ppm), and H-5 (3.76 ppm), respectively. Combined with the HSQC spectrum of RLMP-1, the corresponding signals at 4.13/82.62 ppm, 3.87/77.97 ppm, 4.06/85.22 ppm, and 3.76/62.64 ppm are assigned to the H-2/C-2, H-3/C-3, H-4/C-4, and H-5/C-5, respectively, of α-L-Araf-(1→. Similarly, the chemical shifts at H-2/C-2–H-6/C-6 (H-5/C-5) of the other sugar residues were deduced and assigned. Detailed chemical shift assignments are summarized in Table 6.

The anomeric carbon signals, correspondingly labeled as A, B, D, E, F, G, I, J, K, and L, were identified. Determination of the linking sequence between sugar residues was conducted using the HMBC and NOESY spectra. In the HMBC long-range correlation spectrum, the coupling signal of the anomeric hydrogen with the carbon on each sugar residue or that between the head carbon and hydrogen on each sugar residue facilitated this determination. NOESY serves as a supplementary tool to COSY to complete the assignment of chemical shifts in hydrogen signals within sugar residues, enabling the determination of the connection sequence between two sugar residues based on the cross peak between the anomeric hydrogen of one residue and the hydrogen on the connected carbon of another residue. The HMBC long-range correlation spectrum and the NOESY spectrum were instrumental in inferring the interconnection sequence among various sugar residues. As shown in the HMBC correlation spectrum (Fig. 3G) and NOESY spectrum (Fig. 3F) of the polysaccharide sample, the following coupling signals were found:

Main chain analysis.

A cross peak at δ 4.64/80.16 ppm was detected. The shift at δ 4.64 ppm corresponds to the H-1 of residue E, and that at δ 80.16 ppm corresponds to the C-4 of residue F, suggesting that the backbone of RLMP-1 contains →4)-β-D-Manp-(1 → 4)-β-D-Glcp-(1→. In the NOESY spectrum, the anomeric hydrogen H-1 (δ 4.41 ppm) and H-4 (δ 3.59 ppm) of the sugar residue F showed related signal peaks (F H-1/F H-4), indicating the presence of →4)-β-D-Glcp-(1 → 4)-β-D-Glcp-(1→. The anomeric hydrogen H-1 (δ 4.41 ppm) of sugar residue F and H-6 (δ 4.18 ppm) of sugar residue I showed a related signal peak (F H-1/I H-6), indicating the presence of →4)-β-D-Glcp-(1 → 4,6)-β-D-Glcp-(1 → link.

Side chain analysis.

The cross peak at δ 5.0/68.27 ppm showed the correlation between the H-1 of residue A and the C-5 of residue B, indicating the branching of α-L-Araf-(1 → 5)-α-L-Araf-(1→. In the NOESY spectrum, the cross-peak H-1/ H-6 (4.55/4.18 ppm) presented relevance to the H-1 (δ 4.55 ppm) of the sugar residue J and H-6 (δ 4.18 ppm) of sugar residue I,

indicating the sequences of β-D-Glcp-1 → 4,6)-β-D-Glcp-(1→. The cross-peak H-1/ H-3 (5.15/3.81 ppm) presented the relevance to H-1 (δ 5.15 ppm) of sugar residue D and sugar residue J H-3 (δ 3.81 ppm) and the presence of α-L-Araf-(1 → 3)-β-D-Galp-(1→. The cross-peak H-1/ H-6 (5.15/3.96 ppm) presented the relevance to H-1 (δ 5.15 ppm) of sugar residue D and sugar residue L H-6 (δ 3.96 ppm) and the presence of α-L-Araf-(1 → 3,6)-β-D-Galp-(1 → .

Analysis of main chain and branch chain connections.

In the NOESY spectrum, the anomeric hydrogen H-1 (δ 5.08 ppm) of the sugar residue B and H-6 (δ 4.18 ppm) of the sugar residue I showed related signal peaks (B H-1/I H-6), indicating the presence of →5)-α-L-Araf-(1 → 4,6)-β-D-Glcp-(1→. The anomeric hydrogen H-1 (δ 4.27 ppm) of the sugar residue K and H-6 (δ 4.18 ppm) of the sugar residue I showed related signal peaks (K H-1/I H-6), indicating the presence of →6)-β-D-Galp-(1 → 4,6)-β-D-Glcp-(1→. The anomeric hydrogen H-1 (δ 4.55 ppm) of the sugar residue J and H-6 (δ 4.18 ppm) of the sugar residue I had related signal peaks (J H-1/I H-6), indicating the presence of β-D-Glcp-(1 → 4,6)-β-D-Glcp-(1 → .

In summary, the polysaccharide mainly consists of monosaccharides Glu, Man, Gal, and Ara, and its main glycosidic bond structure is →4)-β-D-Manp-(1 → 4)-β-D-Glcp-(1→4)-β-D-Glcp-(1 → 4)-β-D-Glcp-(1 → 4)-β-D-Glcp- (1 → 4)-β-D-Glcp-(1 → glycosidic bond. Moreover, branched Ara, Glc, and Gal fragments are connected to the main chain via the O-6 bond of →4,6)-β-D-Glcp-(1 → (Fig. 4).

Table 6. Chemical shifts of resonances in the $^{1}H$ and $^{13}C$ NMR spectra of RLMP-1.

### 3.5.6. SEM and TEM

Fig. 5A–C revealed distinct morphological features among the three samples. RLMP-1 exhibited large, irregular particles with a crumbly texture, while RLMP-2 had rough, uneven surfaces composed of sponge-like particles. The RLMP's structure appeared sheet-like and fibrous, with the presence of some thin debris. These observed changes in the apparent structure of the polysaccharides suggest that ultrasonic processing can degrade and modify glycosidic bonds, thereby affecting their overall structural characteristics.

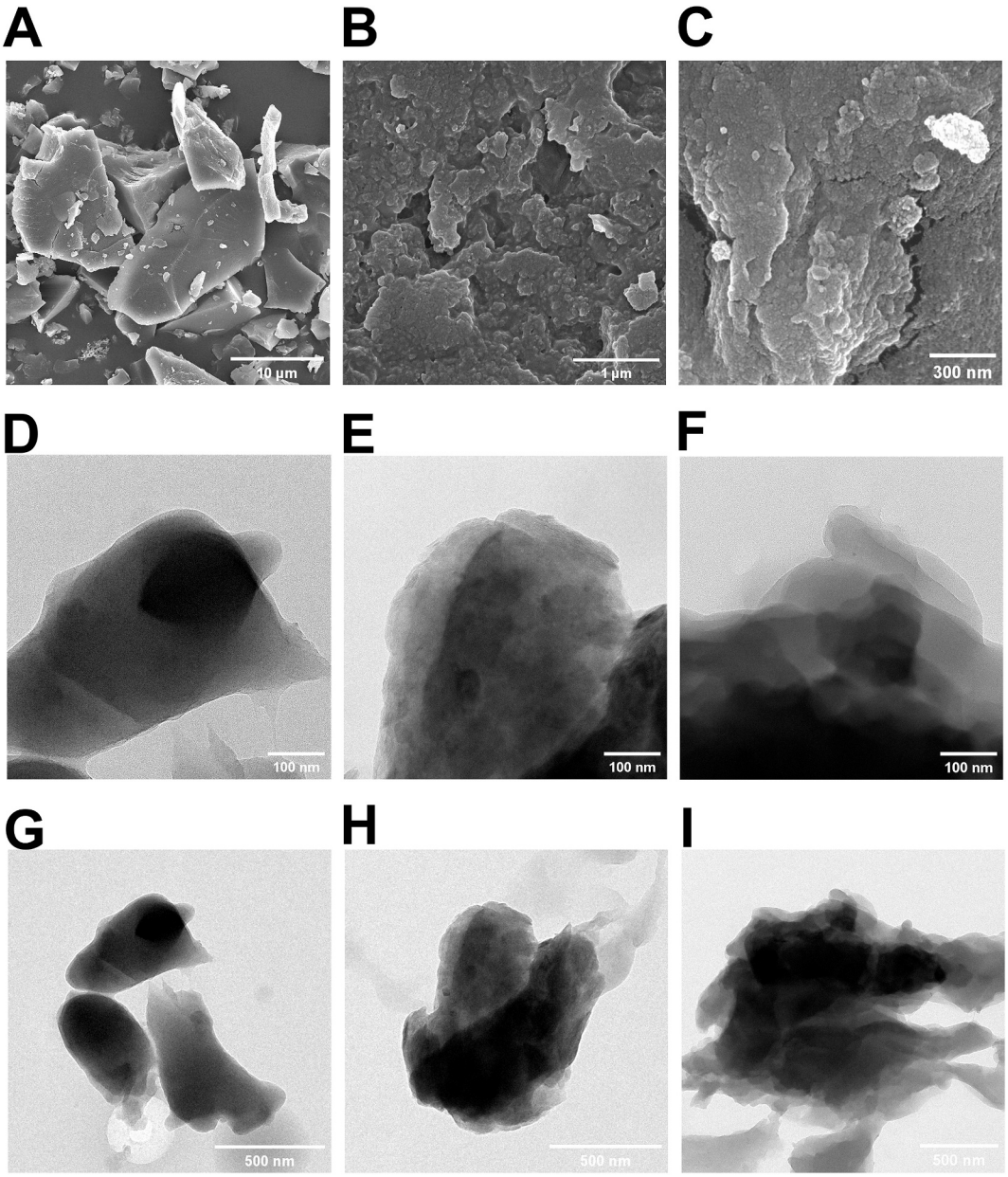


**Fig. 5.** SEM images of RLMP (A), RLMP-1 (B) and RLMP-2 (C); TEM images of RLMP (D, G), RLMP-1 (E, H) and RLMP-2 (F, I).

The conformations of RLMP, RLMP-1, and RLMP-2 were verified by TEM. Following ultrasonic processing, RLMP formed larger aggregates (Fig. 5 D—I). Notably, the structures of RLMP-1 and RLMP-2 closely resembled that of RLMP, suggesting that purification had minimal effect on the internal structure of the polysaccharides.

### 3.6. Hypoglycemic activity

#### 3.6.1. α-Glucosidase inhibitory activity

It can be seen from Fig. 6A that RLMP, RLMP-1, and RLMP-2 inhibited α-glucosidase in a concentration-dependent manner within a range of 25–95 μg/mL. RLMP showed an IC50 value of 38.72 μg/mL, slightly different from that of acarbose (31.09 μg/mL). These findings suggest that RLMP is a promising candidate for developing antidiabetic drugs.

#### 3.6.2. Cytotoxicity assay

When a drug is added at a certain concentration and the cell viability decreases to below 80 % compared to the control group, this suggests potential cytotoxicity at that concentration [14]. Fig. 6B shows the results of the toxicity test on HepG2 cells treated with varying concentrations of RLMP. After 24 h of treatment with RLMP at concentrations of 0.1, 0.3, andd 0.6 mg/mL, cell viability remained above 80 %. This suggests that RLMP does not exhibit significant toxic effects on HepG2 cells within the concentration range of 0.1–0.6 mg/mL.

#### 3.6.3. Glc consumption

As shown in Fig. 6C, glucose consumption in the model group was significantly lower (0.847 mM) than that in the normal group (2.771 mM), indicating the successful establishment of the model. RLMP's effect on the glucose consumption of IR-HepG2 cells compared to model cells was dose-dependent. At an RLMP concentration of 0.6 mg/mL, glucose consumption increased to 2.125 mM, reaching up to 2.226 mM in the normal group. This indicates that RLMP has the ability to improve glucose metabolism in HepG2 cells.

#### 3.6.4. Intracellular glycogen content

As shown in Fig. 6D, the hepatic glycogen content in the model group was significantly lower than that in the normal group ($p < 0.05$). Compared to that of the model cells, the glycogen content of IR-HepG2 cells treated with RLMP was significantly elevated in a dose-dependent manner. At an RLMP concentration of 0.6 mg/mL, the glycogen content increased to 41.938 ± 0.963 (μg/mg prot), compared to the model group ($p < 0.05$), suggesting that RLMP can promote glycogen synthesis, potentially improving hepatic insulin sensitivity.

#### 3.6.5. HK and PK activities

As shown in Fig. 6E-F, the activities of HK and PK in the cells of the model group decreased by 48.92 % and 52.21 %, respectively, compared to those in the cells of the control group. Treatment of IR-HepG2 cells with different concentrations of RLMP resulted in a significant enhancement of intracellular HK and PK activities in all treatment groups, compared to the model group. Notably, when the concentration of RLMP was 0.6 mg/mL, the HK and PK activities were elevated by 70.46 % and 74.02 %, respectively, compared to the model group. The present study demonstrated that RLMP promotes glycolysis and glucose metabolism.

### 3.7. In vitro antioxidant activity

#### 3.7.1. ROS levels

The effect of RLMP on the ROS levels in IR-HepG2 cells is shown in Fig. 7A. Intracellular ROS levels increased significantly in the model group, compared to the normal group. However, treatment with different concentrations of RLMP (0.1, 0.3, and 0.6 mg/mL) resulted in varying degrees of reduction in ROS levels, which decreased with an

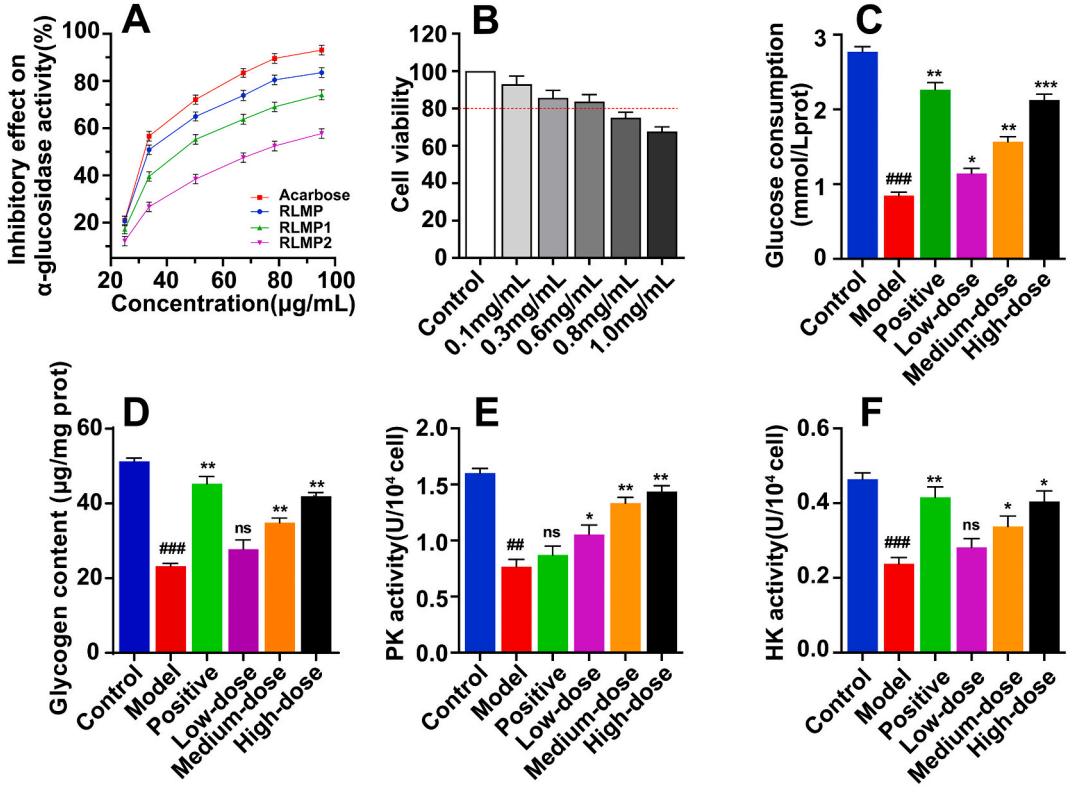


**Fig. 6.** α-Glucosidase inhibitory activity of RLMP, RLMP-1 and RLMP-2 (A). Cell viability of HepG2 (B). Glucose consumption, glycogen content, HK and PK activity of RLMP (C—F). *$p < 0.05$, **$p < 0.01$, ***$p < 0.001$ vs. Model. ##$p < 0.01$, ###$p < 0.001$ vs. Control. The data shown are means ± SD.

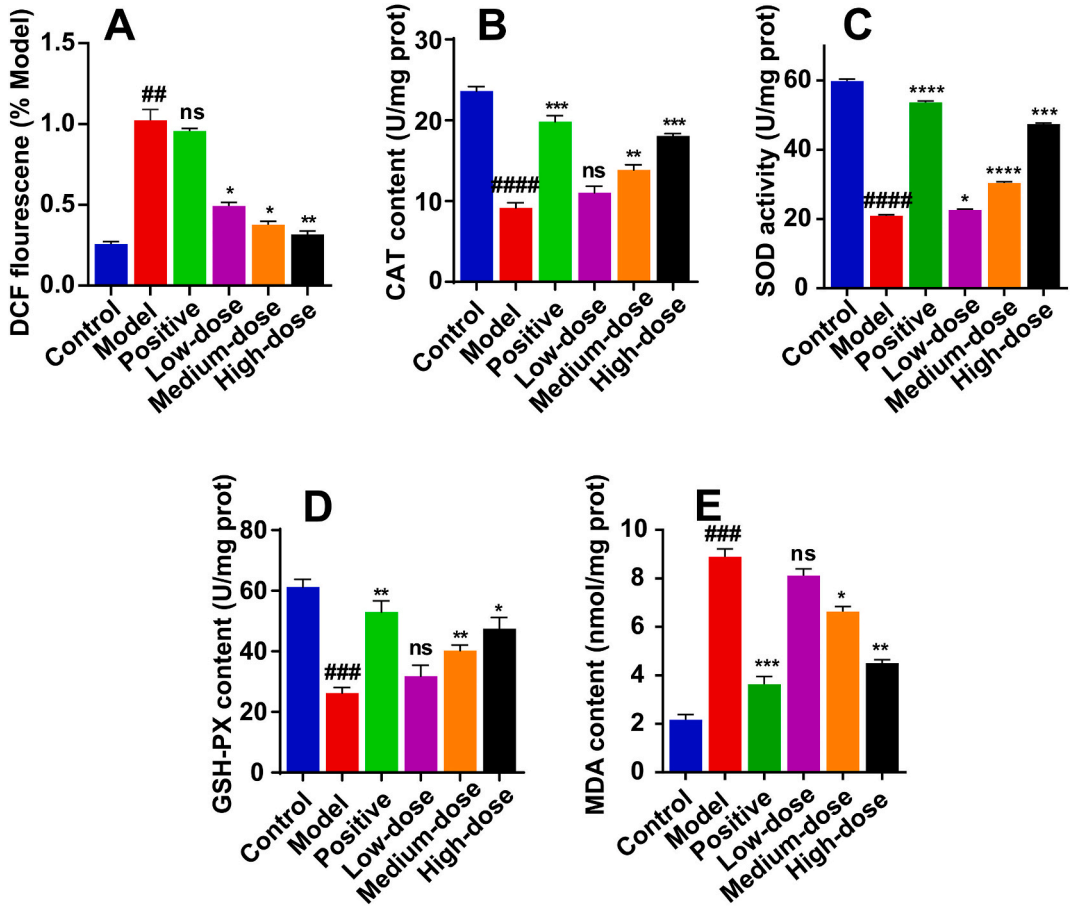


**Fig. 7.** Effects of RLMP on ROS generation (A), CAT (B), SOD (C) and GFH-Px (D) activity, MDA content (E). * $p < 0.05$, ** $p < 0.01$, *** $p < 0.001$ vs. Model. ### $p < 0.001$, #### $p < 0.0001$ vs. Control. The data shown are means ± SD.

increase in polysaccharide concentration, indicating a dose-dependent effect. At 0.6 mg/mL, RLMP treatment reduced intracellular ROS levels by 63.47 %, compared to the model group, demonstrating its potential to inhibit ROS production. These findings suggest that RLMP may improve IR by scavenging ROS.

### *3.7.2. CAT, SOD, and GSH-Px activities and MDA levels*

The antioxidant effects of RLMP were assessed by measuring the levels of CAT, SOD, GSH-Px, and MDA in IR-HepG2 cells (Fig. 7B-E). Compared to those in the control group, the CAT, SOD, and GSH-Px activities in IR-HepG2 cells were reduced by 62.41 %, 65.02 %, and 57.09 %, respectively, whereas the MDA content was increased by 75.6 %, indicating enhanced oxidative stress. Pretreatment with RLMP effectively mitigated oxidative damage in a concentration-dependent manner, as evidenced by the increased activities of intracellular antioxidant enzymes. Compared to the model group, continuous administration of RLMP increased the activities of CAT, SOD, and GSH-Px by 20.4–97.4 %, 8.2–126.6 % and 21.1–80.7 %, respectively, but decreased that of MDA by 8.8–49.3 %. These results indicate that RLMP can protect antioxidant enzymes from oxidative stress-induced damage, thereby reducing cellular damage.

### *3.8. Expression of related proteins*

As shown in Fig. 8A–D, the levels of PI3K, p-AKT, and GLUT4 was markedly reduced in the model group, compared to the control group ($p < 0.05$). Conversely, there was a significant increase in that of p-IRS-1 in the model group, compared to the control group ($p < 0.05$), suggesting that insulin signaling was blocked, eventually leading to endothelial cell injury and IR. After treatment with RLMP, the levels of p-PI3K, p-AKT, and GLUT4 was significantly enhanced, especially in the high-dose group, with substantial increases of 73.2 %, 76.5 %, and 56.9 %, respectively. Conversely, there was a notable decrease of 65.6 % in p-IRS-1 expression. There were no significant differences in the protein levels of Akt, PI3K, and IRS-1 across the control, model, and treatment groups ($p > 0.05$) groups, suggesting that regulation of p-PI3K-, p-AKT-, p-IRS-1-, and GLUT4-related protein levels may be involved in modulating the hypoglycemic effect of RLMP.

## 4. Discussion

Ultrasonic vibration generates cavitation bubbles, which not only accelerate tissue rupture but also enhance mass transfer. Meanwhile, microwave radiation is highly penetrating and can cause a rapid increase in internal temperature, leading to a sharp rise in intracellular pressure, thereby intensifying the effects of ultrasonication and reducing extraction time. Therefore, the combination of ultrasound and microwave radiation can leverage their respective advantages. As a result, the polysaccharide yield of UMAE is expected to be higher than that of HRE, UAE, and MAE. Zhang et al. [21] obtained similar results using the UMAE method. In this study, it was confirmed that the RLMP yield of UMAE was indeed significantly higher than that of HRE, UAE, and MAE. Thus, UMAE is the most effective method for polysaccharide extraction from RLM.

The bioactivities of polysaccharides are closely associated with their structural characteristics, including monosaccharide composition, molecular weight, and types of glycosyl linkages. Previous studies have reported the isolation of two polysaccharides from the fruit of *Rosa*

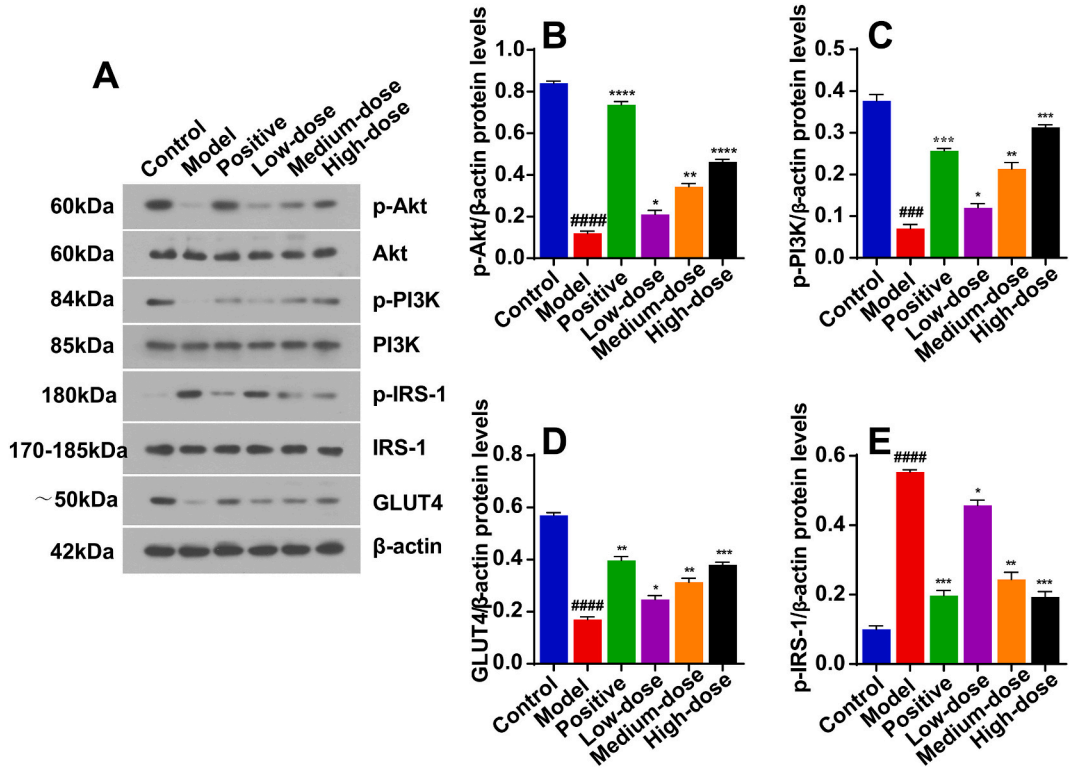


**Fig. 8.** Western blot analysis of expression levels of p-Akt, p-PI3K, GLUT4 proteins and p-IRS-1 in HepG2-IR cells after treatment by different concentrations of RLMP (A); Quantitative analysis of relative expression of p-Akt/β-actin (B), p-PI3K/β-actin (C), GLUT4/β-actin proteins (D) and p-IRS-1/β-actin (E). Model group: IR, Positive group: MET, others were RLMP at different concentrations (Low dose: 0.1 mg/mL, Medium dose: 0.3 mg/mL, High dose: 0.6 mg/mL) group. * $p < 0.05$, ** $p < 0.01$, *** $p < 0.001$, **** $p < 0.0001$ vs. Model. ### $p < 0.001$, #### $p < 0.0001$ vs. Control. The data shown are means ± SD.

*laevigata*, with monosaccharide compositions of mannose, glucose, galactose, and xylose, and mannose, rhamnose, glucose, galactose, and xylose, respectively. Both polysaccharides exhibited antioxidant and neuroprotective effects [11]. In this study, our results indicate that Ara, Glc, and Gal are the most abundant monosaccharides in RLMP obtained via UMAE. The literature has confirmed that polysaccharides with higher Ara or Xyl content exhibit significant inhibitory effects on α-glucosidase activity [34,43]. Therefore, the hypoglycemic activity of RLMP may be attributed to its high arabinose content.

Glycogen, a key indicator of glucose metabolism, is the primary storage form of glucose in the body. Impaired glycogen synthesis contributes to hyperglycemia. Promoting synthesis is essential for reducing blood glucose levels and preventing complications [44,45]. In present study, a significant decrease in glycogen content was observed in the model group, and this was restored following RLMP treatment. IR often causes decreased glucose consumption and the suppressed activity of enzymes involved in hepatic glycolysis, such as HK and PK. Decreased HK and PK activities in hepatocytes lead to reduced glycogen synthesis, decreased glucose consumption, and disturbed glucose metabolism, ultimately affecting blood glucose levels. In this study, the HK and PK activities in IR-HepG2 cells were significantly increased following RLMP treatment, suggesting that RLMP exerts an ameliorative effect on hyperglycemia, the mechanism of which is likely related to enhanced glucose metabolism and an increase in glycogen content. Similar results have been reported that polysaccharides extracted from *Lycium barbarum* fruit significantly increased the activities of HK and PK in the livers of diabetic animals [46].

Oxidative stress may lead to β-cell dysfunction and glycemic abnormalities, which are important mechanisms for inducing IR. Elevated levels of ROS and decreased activity of antioxidants are major contributors to oxidative stress. Increased oxidative stress in vivo impairs insulin sensitivity and disrupts the regulation of glucose uptake by interfering with insulin signaling in hepatocytes [47,48]. Based on these findings, we investigated the levels of ROS and MDA and the activities of intracellular antioxidant enzymes, namely CAT, SOD, and GSH-Px, in IR-HepG2 cells. The results showed that IR-HepG2 cells had significantly increased ROS and MDA levels but decreased CAT, SOD, and GSH-Px activities, reflecting increased oxidative stress. Treatment with different concentrations of RLMP decreased ROS levels and enhanced CAT, SOD, and GSH-Px activities in IR-HepG2 cells, suggesting that RLMP exerts antioxidant effects by regulating the activities of antioxidant enzymes and glutathione metabolism, thereby reducing IR and alleviating diabetes.

IRS-1 is a docking protein for the insulin receptor and is widely expressed in mammalian myocytes. IRS-1 activates the phosphorylation of PI3K and the downstream kinase Akt, which is essential for activating the downstream PI3K/Akt signaling pathway. PI3K activation regulates glucose uptake, and Akt is the main signaling substance produced by PI3K activation. The PI3K/Akt signaling pathway regulates insulin-mediated glucose uptake and metabolism [49,50]. Dysregulation of the PI3K/Akt pathway underlies IR in diabetes. GLUT-4, a key glucose transporter, not only transports glucose into adipocytes and muscle cells but also uptakes glucose into the insulin-responsive zone [51]. Therefore, we hypothesized that IR may lead to abnormal glucose metabolism and oxidative stress by disrupting the PI3K/Akt/GLUT-4 pathway and analyzed the effect of RLMP on this pathway. Our findings showed that IRS-1, PI3K, and pAkt protein levels were suppressed in IR-HepG2 cells, compared to normal controls, and RLMP treatment increased their levels. Diabetic stimulation significantly reduced GLUT-4 levels, whereas RLMP treatment significantly increased them. Therefore, RLMP effectively regulates key targets in the PI3K/Akt/GLUT4 signaling pathway, hence improving IR.

## 5. Conclusion

In this study, the optimum extraction process and in vitro hypoglycemic activity of RLMP were investigated. An optimized UMAE method was developed for extracting RLMP, achieving a higher yield than other extraction methods. After the isolation and purification of crude RLMP, RLMP-1 was identified as having a glycosidic bond structure of →4)-β-D-manp-(1 → 4)-β-D-glcp-(1→4)-β-D-glcp-(1 → 4)-β-D-glcp-(1 → 4)-β-D-glcp-(1 → 4)-β-D-glcp-(1 → . Moreover, RLMP significantly improved the levels of glucose-related indicators in insulin-induced HepG2 cells, highlighting its pronounced hypoglycemic activity. The mechanism of action involved the activation of the PI3K/Akt/GLUT-4 signaling pathway, which enhanced glucose metabolism, increased glycogen content, and alleviated oxidative stress. These findings provide a theoretical basis for the potential application of polysaccharides from *Rosa laevigata* in functional foods and antidiabetic drugs.

Supplementary data to this article can be found online at https://doi.org/10.1016/j.ijbiomac.2024.135116.

## CRediT authorship contribution statement

**Shuai Chen:** Writing – original draft, Supervision, Methodology, Funding acquisition, Formal analysis, Conceptualization. **Liang Wang:** Writing – original draft, Investigation. **Shuang Rong:** Visualization, Investigation. **Yuyuan Duan:** Software, Resources. **Huizhu Wang:** Writing – review & editing, Supervision, Resources, Funding acquisition, Conceptualization.

## Declaration of competing interest

The authors declare the following financial interests/personal relationships which may be considered as potential competing interests:

1. Huizhu Wang reports financial support was provided by the Department of Education of Jilin Province.
2. Shuai Chen reports financial support was provided by the Department of Education of Jilin Province.

## Acknowledgments

This work received financial support from the Science and Technology Project of the Department of Education of Jilin Province (accession number: JJKH20200256KJ) and the Science and Technology Project of the Department of Education of Jilin Province (accession number: JJKH20190824KJ).

## References

[1] L. He, P. Huan, J. Xu, Y. Chen, L. Zhang, J. Wang, L. Wang, Z. Jin, Hedysarum polysaccharide alleviates oxidative stress to protect against diabetic peripheral neuropathy via modulation of the keap1/Nrf2 signaling pathway, J. Chem. Neuroanat. 126 (2022) 102182, https://doi.org/10.1016/j.jchemneu.2022.102182.

[2] N. Zhou, Y. Zhao, L. Zhang, Y. Ning, Protective effects of black onion polysaccharide on liver and kidney injury in T2DM rats through the synergistic impact of hypolipidemic and antioxidant abilities, Int. J. Biol. Macromol. 223 (2022) 378–390, https://doi.org/10.1016/j.ijbiomac.2022.11.055.

[3] C. Cao, B. Zhang, C. Li, Q. Huang, X. Fu, R.H. Liu, Structure and in vitro hypoglycemic activity of a homogenous polysaccharide purified from Sargassum pallidum, Food Funct. 10 (2019) 2828–2838, https://doi.org/10.1039/c8fo02525h.

[4] Z. Zhang, Q. Zhang, X. Huang, K. Luo, Intestinal microbiology and metabolomics of streptozotocin-induced type 2 diabetes mice by polysaccharide from Cardamine violifolia, J. Funct. Foods 97 (2022) 105251, https://doi.org/10.1016/j.jff.2022.105251.

[5] X. Ji, J. Guo, T. Cao, T. Zhang, Y. Liu, Y. Yan, Review on mechanisms and structure-activity relationship of hypoglycemic effects of polysaccharides from natural resources, Food Sci. Human Wellness 12 (2023) 1969–1980, https://doi.org/10.1016/j.fshw.2023.03.017.

[6] Z. Jiang, Y. Wang, D. Xiang, Z. Zhang, Structural properties, antioxidant and hypoglycemic activities of polysaccharides purified from pepper leaves by high-speed counter-current chromatography, J. Funct. Foods 89 (2022) 104916, https://doi.org/10.1016/j.jff.2021.104916.

[7] Y. Cai, Z. Si, Y. Jiang, M. Ye, F. Wang, X. Yang, J. Yu, X. Gao, W. Liu, Structure-activity relationship of low molecular weight Astragalus membranaceus polysaccharides produced by Bacteroides, Carbohydr. Polym. 316 (2023) 121036, https://doi.org/10.1016/j.carbpol.2023.121036.

[8] A.F. El Sheikha, Biotechnology and production of anti-cancer compounds, in: S. Malik (Ed.), Medicinal Plants: Ethno-Uses to Biotechnology Era, Springer International Publishing AG. Part of Springer Nature, Cham, Switzerland, 2017, pp. 1–38, https://doi.org/10.1007/978-3-319-53880-8_1.

[9] K.J.S. Kumar, C. Lin, Y.H. Tseng, S.Y. Wang, Fruits of Rosa laevigata and its bioactive principal sitostenone facilitate glucose uptake and insulin sensitivity in hepatic cells via AMPK/PPAR-γ activation, Phytomedicine Plus 1 (2021) 100109, https://doi.org/10.1016/j.phyplu.2021.100109.

[10] D. Dong, S. Zhang, L. Yin, X. Tang, Y. Xu, X. Han, Y. Qi, J. Peng, Protective effects of the total saponins from Rosa laevigata Michx fruit against carbon tetrachloride-induced acute liver injury in mice, Food Chem. Toxicol. 62 (2013) 120–130, https://doi.org/10.1016/j.fct.2013.08.050.

[11] X. Liu, Y. Gao, D. Li, C. Liu, M. Jin, J. Bian, M. Lv, Y. Sun, L. Zhang, P. Gao, The neuroprotective and antioxidant profiles of selenium-containing polysaccharides from the fruit of Rosa laevigata, Food Funct. 9 (2018) 1800–1808, https://doi.org/10.1039/c7fo01725a.

[12] J. Zhang, Z. Song, Y. Li, S. Zhang, J. Bao, H. Wang, C. Dong, Y. Ohizumi, J. Xu, Y. Guo, Structural analysis and biological effects of a neutral polysaccharide from the fruits of Rosa laevigata, Carbohydr. Polym. 265 (2021) 118080, https://doi.org/10.1016/j.carbpol.2021.118080.

[13] X. Zhang, Y. Hu, C. Jin, W. Wu, Extraction and hypolipidemic activity of low molecular weight polysaccharides isolated from Rosa laevigata fruits, Biomed. Res. Int. 2020 (2020) 2043785, https://doi.org/10.1155/2020/2043785.

[14] X. Liu, J. Liu, C. Liu, X. Zhang, Z. Zhao, J. Xu, X. Zhang, K. Zhou, P. Gao, D. Li, Selenium-containing polysaccharides isolated from *Rosa laevigata* Michx fruits exhibit excellent anti-oxidant and neuroprotective activity in vitro, Int. J. Biol. Macromol. 209 (2022) 1222–1233, https://doi.org/10.1016/j.ijbiomac.2022.04.146.

[15] J.K. Yan, T.T. Chen, Z.W. Wang, C. Wang, C. Liu, L. Li, Comparison of physicochemical characteristics and biological activities of polysaccharides from barley (Hordeum vulgare L.) grass at different growth stages, Food Chem. 389 (2022) 133083, https://doi.org/10.1016/j.foodchem.2022.133083.

[16] S. Shen, C. Zhou, Y. Zeng, H. Zhang, M.A. Hossen, J. Dai, S. Li, W. Qin, Y. Liu, Structures, physicochemical and bioactive properties of polysaccharides extracted from Panax notoginseng using ultrasonic/microwave-assisted extraction, Lwt 154 (2022) 112446, https://doi.org/10.1016/j.lwt.2021.112446.

[17] Z. Wang, X. Zhou, L. Sheng, D. Zhang, X. Zheng, Y. Pan, X. Yu, X. Liang, Q. Wang, B. Wang, N. Li, Effect of ultrasonic degradation on the structural feature, physicochemical property and bioactivity of plant and microbial polysaccharides: a review, Int. J. Biol. Macromol. 236 (2023) 123924, https://doi.org/10.1016/j.ijbiomac.2023.123924.

[18] J. Yang, S. Dong, X. Zhou, W. Zhang, Y. Gu, L. Zheng, G. Yang, J. Wang, Y. Zhang, Polysaccharides from waste Zingiber mioga leaves: ultrasonic-microwave-assisted extraction, characterization, antioxidant and anticoagulant potentials, Ultrason. Sonochem. 101 (2023) 106718, https://doi.org/10.1016/j.ultsonch.2023.106718.

[19] M. Oroian, F. Dranca, F. Ursachi, Comparative evaluation of maceration, microwave and ultrasonic-assisted extraction of phenolic compounds from propolis, J. Food Sci. Technol. 57 (1) (2019) 70–78, https://doi.org/10.1007/s13197-019-04031-x.

[20] H. Sun, C. Li, Y. Ni, L. Yao, H. Jiang, X. Ren, Y. Fu, C. Zhao, Ultrasonic/microwave-assisted extraction of polysaccharides from Camptotheca acuminata fruits and its antitumor activity, Carbohydr. Polym. 206 (2019) 557–564, https://doi.org/10.1016/j.carbpol.2018.11.010.

[21] Y. Zhang, Y. Lei, S. Qi, M. Fan, S. Zheng, Q. Huang, X. Lu, Ultrasonic-microwave-assisted extraction for enhancing antioxidant activity of Dictyophora indusiata polysaccharides: the difference mechanisms between single and combined assisted extraction, Ultrason. Sonochem. 95 (2023) 106356, https://doi.org/10.1016/j.ultsonch.2023.106356.

[22] H. Wang, N. Wang, L. Ma, D. Pei, D. Di, J. Liu, Polysaccharides from different cultivars of wolfberry: physicochemical characteristics and protection against oxidative stress, Ind. Crop. Prod. 197 (2023) 116548, https://doi.org/10.1016/j.indcrop.2023.116548.

[23] M. Fang, Z. Yu, W. Zhang, J. Cao, W. Liu, Friction coefficient calibration of corn stalk particle mixtures using Plackett-Burman design and response surface methodology, Powder Technol. 396 (2022) 731–742, https://doi.org/10.1016/j.powtec.2021.10.040.

[24] R. Venkataraghavan, R. Thiruchelvi, D. Sharmila, Statistical optimization of textile dye effluent adsorption by Gracilaria edulis using Plackett-Burman design and response surface methodology, Heliyon 6 (2020) e05219, https://doi.org/10.1016/j.heliyon.2020.e05219.

[25] J. Tan, P. Cui, S. Ge, X. Cai, Q. Li, H. Xue, Ultrasound assisted aqueous two-phase extraction of polysaccharides from Cornus officinalis fruit: modeling, optimization, purification, and characterization, Ultrason. Sonochem. 84 (2022) 105966, https://doi.org/10.1016/j.ultsonch.2022.105966.

[26] H. Xue, W. Wang, J. Wu, K. Xie, S. Ge, J. Tan, Ultrasound assisted aqueous two-phase extraction of polysaccharides from corn stigma: process optimization, structure characterization, and immunomodulatory activity, Innov. Food Sci. Emerg. Technol. 91 (2024) 103531, https://doi.org/10.1016/j.ifset.2023.103531.

[27] N. Shende, A. Karale, P. Bore, S. Bhagade, A. Gulhane, A.D. Mallya, R.M. Dhere, Evaluation of structural modification induced activation of pneumococcal polysaccharide by GC-MS for the conjugate vaccine, Carbohydr. Res. 531 (2023) 108878, https://doi.org/10.1016/j.carres.2023.108878.
[28] H. Xue, J. Xu, J. Zhang, Y. Wei, X. Cai, J. Tan, Modeling, optimization, purification, and characterization of polysaccharides from Lilium lancifolium Thunb, LWT 162 (2022) 113491, https://doi.org/10.1016/j.lwt.2022.113491.
[29] A.K. Giri, P.C. Mishra, Optimization of different process parameters for the removal efficiency of fluoride from aqueous medium by a novel bio-composite using Box-Behnken design, J. Environ. Chem. Eng. 11 (2023) 109232, https://doi.org/10.1016/j.jece.2022.109232.
[30] S. Zhou, G. Huang, Extraction, structural analysis and antioxidant activity of aloe polysaccharide, J. Mol. Struct. 1273 (2023) 134379, https://doi.org/10.1016/j.molstruc.2022.134379.
[31] C.Y. Shen, J.G. Jiang, M.Q. Li, C.Y. Zheng, W. Zhu, Structural characterization and immunomodulatory activity of novel polysaccharides from Citrus aurantium Linn. variant amara Engl, J. Funct. Foods 35 (2017) 352–362, https://doi.org/10.1016/j.jff.2017.05.055.
[32] S. Wang, G. Li, X. Zhang, Y. Wang, Y. Qiang, B. Wang, J. Zou, J. Niu, Z. Wang, Structural characterization and antioxidant activity of Polygonatum sibiricum polysaccharides, Carbohydr. Polym. 291 (2022) 119524, https://doi.org/10.1016/j.carbpol.2022.119524.
[33] W. Cai, K. Wong, Q. Huang, Isolation, structural features, rheological properties and bioactivities of polysaccharides from Lignosus rhinocerotis: a review, Int. J. Biol. Macromol. 242 (2023) 124818, https://doi.org/10.1016/j.ijbiomac.2023.124818.
[34] Z. Chen, Y. Liu, D. Wang, N. Wu, K. Wang, Y. Zhang, Preparation, chemical structure and α-glucosidase inhibitory activity of sulfated polysaccharide from Grifola frondosa, J. Funct. Foods 98 (2022) 105289, https://doi.org/10.1016/j.jff.2022.105289.
[35] Y. Wang, Y. Zhang, J. Cheng, J. Zhao, R. Shi, L. He, Q. Li, Y. Chen, Efficient purification of flavonoids from bamboo shoot residues of Phyllostachys edulis by macroporous resin and their hypoglycemic activity, Food Chem. X 16 (2022) 100505, https://doi.org/10.1016/j.fochx.2022.100505.
[36] C. Cao, C. Li, Q. Chen, Q. Huang, M.E.M. Pérez, X. Fu, Physicochemical characterization, potential antioxidant and hypoglycemic activity of polysaccharide from Sargassum pallidum, Int. J. Biol. Macromol. 139 (2019) 1009–1017, https://doi.org/10.1016/j.ijbiomac.2019.08.069.
[37] Y. Yu, J. Nie, B. Zhao, J. Tan, C. Lv, J. Lu, Structure characterization and anti-fatigue activity of an acidic polysaccharide from Panax ginseng C. A. Meyer, J. Ethnopharmacol. 301 (2023) 115831, https://doi.org/10.1016/j.jep.2022.115831.
[38] H. Hao, C. Cui, Y. Xing, X. Jia, B. Ma, W. Kang, T. Li, M. Gao, C. Xu, Sulfation of the extracellular polysaccharide from the edible fungus Stropharia rugosoannulata with its antioxidant activity, J. Future Foods 3 (2023) 37–42, https://doi.org/10.1016/j.jfutfo.2022.09.006.
[39] Y. Zhu, J. Lv, Y. Gu, Y. He, J. Chen, Z. Zhou, X. Ye, Polysaccharides of Chinese bayberry pomace wine: structural characteristics, antioxidant activity and influence on the bayberry wine, Food Biosci. 50 (2022) 102025, https://doi.org/10.1016/j.fbio.2022.102025.
[40] L. Pan, L. Wang, F. Zhang, Y. Zhang, B. Zheng, Structural characterization and bifidogenic activity of polysaccharide from Dictyophora indusiata, Food Biosci. 51 (2023) 102297, https://doi.org/10.1016/j.fbio.2022.102297.
[41] Y. Zheng, A. Mort, Isolation and structural characterization of a novel oligosaccharide from the rhamnogalacturonan of Gossypium hirsutum L, Carbohydr. Res. 343 (2008) 1041–1049, https://doi.org/10.1016/j.carres.2008.02.021.
[42] X. Wang, M. Zhang, D. Zhang, X. Wang, H. Cao, Q. Zhang, C. Yan, Structural elucidation and antiosteoporosis activities of polysaccharides obtained from Curculigo orchioides, Carbohydr. Polym. 203 (2019) 292–301, https://doi.org/10.1016/j.carbpol.2018.09.059.
[43] Q.Q. Lv, J.J. Cao, R. Liu, H.Q. Chen, Structural characterization, α-amylase and α-glucosidase inhibitory activities of polysaccharides from wheat bran, Food Chem. 341 (2021) 128218, https://doi.org/10.1016/j.foodchem.2020.128218.
[44] S.Z. Xie, W.J. Zhang, W. Liu, J.B. Bai, S.L. Xie, T. Wang, G.B. Xu, D.L. Wu, Physicochemical characterization and hypoglycemic potential of a novel polysaccharide from Polygonatum sibiricum red through PI3K/Akt mediated signaling pathway, J. Funct. Foods 93 (2022) 105080, https://doi.org/10.1016/j.jff.2022.105080.
[45] L. Miao, H. Zhang, M.S. Cheong, R. Zhong, P. Garcia-Oliveira, M.A. Prieto, K. W. Cheng, M. Wang, H. Cao, S. Nie, J. Simal-Gandara, W.S. Cheang, J. Xiao, Anti-diabetic potential of apigenin, luteolin, and baicalein via partially activating PI3K/Akt/Glut-4 signaling pathways in insulin-resistant HepG2 cells, Food Sci. Human Wellness 12 (6) (2023) 1991–2000, https://doi.org/10.1016/j.fshw.2023.03.021.
[46] J. Zhu, W. Liu, J. Yu, S. Zou, J. Wang, W. Yao, X. Gao, Characterization and hypoglycemic effect of a polysaccharide extracted from the fruit of Lycium barbarum L, Carbohydr. Polym. 98 (2013) 8–16, https://doi.org/10.1016/j.carbpol.2013.04.057.
[47] E. Rendra, V. Riabov, D.M. Mossel, T. Sevastyanova, M.C. Harmsen, J. Kzhyshkowska, Reactive oxygen species (ROS) in macrophage activation and function in diabetes, Immunobiology 224 (2019) 242–253, https://doi.org/10.1016/j.imbio.2018.11.010.
[48] Q. Shi, X. Li, J. He, D. Ye, H. Tang, J. Xuan, Y. Tang, Y. Zhang, Y. Zhang, Effects of Auricularia auricula-judae (Bull.) Quél. polysaccharide acid hydrolysate on glucose metabolism in diabetic mice under oxidative stress, Phytomedicine 128 (2024) 155485, https://doi.org/10.1016/j.phymed.2024.155485.
[49] B.O. Ajiboye, C.D. Famusiwa, M.O. Amuda, S.O. Afolabi, B.T. Ayotunde, A. A. Adejumo, A.F.I. Akindele, B.E. Oyinloye, O.V. Owolabi, C. Genovese, O.A. Ojo, Attenuation of PI3K/AKT signaling pathway by Ocimum gratissimum leaf flavonoid-rich extracts in streptozotocin-induced diabetic male rats, Biochem. Biophys. Rep. 38 (2024) 101735, https://doi.org/10.1016/j.bbrep.2024.101735.
[50] H. Xue, Z. Hao, Y. Gao, X. Cai, J. Tang, X. Liao, J. Tan, Research progress on the hypoglycemic activity and mechanisms of natural polysaccharides, Int. J. Biol. Macromol. 252 (2023) 126199, https://doi.org/10.1016/j.ijbiomac.2023.126199.
[51] Y. Zhu, Z. He, X. Bao, M. Wang, S. Yin, L. Song, Q. Peng, Purification, in-depth structure analysis and antioxidant stress activity of a novel pectin-type polysaccharide from Ziziphus Jujuba cv. Muzaoresidue, J. Funct. Foods 80 (2021) 104439, https://doi.org/10.1016/j.jff.2021.104439.